Master Thesis

A computational study of the single cell and network properties differentiating the response of mitral and tufted cells of the olfactory bulb

Author: Eleni Genitsaridi

Supervisor: Panayiota Poirazi, Ph.D.

University of Crete, Faculty of Medicine

Heraklion, Greece

A thesis submitted in fulfillment of the requirements for the degree of Master in "Neuroscience".

March 2016

Abstract

Olfactory perception is an important sense for humans and other animals with unique characteristics. Odor related information is transduced by olfactory sensory neurons located in the nasal epithelium and this information is transmitted to the olfactory bulb. Projection neurons of the olfactory bulb further transmit this information to other brain areas of the olfactory system. The olfactory bulb, however, is not just a relay station. The strict spatial organization, the large number of local interneurons and the diversity of projection neurons are indicative of an active role in the processing of odor information.

Projections neurons of the olfactory bulb can be categorized into two distinct populations, namely the mitral and tufted cells, regarding morphological, biophysical and synaptic properties. Although the existence of distinct subtypes of projection neurons in the olfactory bulb is known for decades, the responsible mechanisms and their functional implications remain elusive. In this study we used in silico models to investigate the role of single-cell and network properties in differentiating the response of mitral and tufted cells to an odor input. Using the NEURON simulation environment we developed two parallel non-overlapping networks of the olfactory bulb, the mitral and the tufted networks. Our results from stimulating the networks with different input patters are in agreement with the view that the two networks use different coding schemes to encode different aspects of odor information.

Acknowledgments

Firstly, I would like to thank my thesis advisor Panayiota Poirazi for the continuous support of my MSc study. Also, I would like to thank both Professor Kiki Thermou and Kiki Sidiropoulou for their participation in my Master's thesis committee. Special thanks go to my post-doc supervisors, Nassi Papoutsi and Constantinos Melachrinos, for all the help and guidance they have offered me. To the rest of my lab-mates, thanks for the fun and support. Last but not least, I would like to thank my family and my friends for everything. And especially Yianni for his artistic contribution.

Eleni Genitsaridi, Heraklion, March 2016

Contents

1 | Introduction

1.1 The Olfactory Bulb

The mammalian olfactory bulb is a neural structure of the central nervous system and constitutes the first relay of the odor-processing pathways. Olfactory receptors located in the nasal epithelium interact with odor molecules and produce signals that are carried to the olfactory bulb by the axons of the olfactory sensory neurons. This information is processed by the local neuronal circuits of the olfactory bulb and, subsequently, the projection neurons transmit the odor signals to other brain areas of the olfactory system (Shepherd et al., 2004). Local interneurons characteristically outnumber projection neurons, unlike most other central nervous system areas (Mori, 2014). They consist of multiple types of neurons (such as periglomerular and granule cells) and they have a prominent role in shaping odor representations (Nagayama et al., 2014).

The projection neurons also comprise a highly diverse population. They can, however, be categorized into two main subpopulations with distinct morphological, biophysical, synaptic and response properties. These are the mitral and the tufted cells. Briefly, compared to tufted cells, mitral cells have larger cell bodies located deeper in the olfactory bulb and extend longer secondary dendrites (Macrides et al., 1985, Nagayama et al., 2014), they are intrinsically less excitable (Burton and Urban, 2014), they respond to odor stimulation with lower frequency and more delayed firing patterns (Fukunaga et al., 2012, Igarashi et al., 2012, Nagayama et al., 2004) and they send axons to both anterior and posterior cortical areas (Igarashi et al., 2012). Regarding the axon distribution, tufted cells innervate mainly anterior regions of the olfactory cortex. Although the diversity even within these populations is high, recent evidence suggest that the axons of mitral and tufted cells form

two generally independent and distinguishable pathways for the transduction of odor signals to the olfactory cortex (Fukunaga et al., 2012, Igarashi et al., 2012, Nagayama et al., 2004).

1.2 Computational Neuroscience

Computational neuroscience refers to the use of computational and mathematical models to study brain functions and neural systems and is part of the field of computational biology. At first, studies of the nervous system used mathematics only in terms of data analysis. The past few decades, however, computational modeling has been used to simulate biological systems, incorporating the essential features of these systems. Computational models can range from models describing nano-scale molecular interactions to models of large-scale neural networks. One of the most important contributions to the field of modeling neural cells was the Hodgkin-Huxley model for the generation of action potentials. For this work Hodgkin and Huxley received the 1963 Nobel Prize in Physiology or Medicine.

Importantly, computational neuroscience works in parallel with experimental neuroscience. Data provided by the latter are used to set up realistic computational models. On the other hand, questions that can not be addressed experimentally, for example due to prohibitive cost or ethical issues, can be dealt with computational methods. Experiments using computational models can generate hypotheses and predictions about the real world. Depending on the question, models of neural networks can either be biophysically realistic compartmental models or large scale networks of simple neuron models. The use of computational neuroscience for describing and elucidating the organization and the functions of the brain has led to numerous important findings during the last decades, including understanding the functionality of sensory systems and the neural basis of learning and memory. In particular, models of the olfactory system have given insight into the signal processing

mechanisms of this system (Cleland and Linster, 2005). With the increasing complexity and quantity of experimental data, the contribution of computational modeling will most probably also increase the following years.

1.3 Overview of this study

Most computational studies of the olfactory bulb to date model the projection neurons as a single cell type, validated with experimental data regarding mitral cell properties (Kaplan and Lansner, 2014, Koulakov and Rinberg, 2011, Li and Cleland, 2013, Yu et al., 2013). Some recent computational studies have incorporated tufted cells in their networks but they use simplified single cell models (Polese et al., 2014), they model the interneuron external tufted cell rather than projecting tufted cells (Carey et al., 2015), or they only change network parameters to differentiate between mitral and tufted networks (Fukunaga et al., 2012). To our knowledge, there is yet no reported biophysical compartmental model of a tufted projection neuron.

Driven by this limitation in the literature, we designed this study to develop two parallel networks of the olfactory bulb, incorporating distinct intrinsic biophysical and network properties for the mitral and the tufted networks. The aim of our study was firstly to investigate the role of single-cell and network properties in differentiating the response of mitral and tufted cells and secondly to predict possible functional roles for this differentiation. Towards this goal, we modified a morphologically simplified biophysical model of a mitral cell (Li and Cleland, 2013) to develop a mitral and a tufted cell model. Both single-cell models were simulated in the NEURON simulation environment and were extensively validated against recently published experimental data regarding the distinct intrinsic biophysical properties of mitral and tufted cells (Burton and Urban, 2014).

After tuning the two cells, we incorporated them into two distinct, non-overlapping networks, the mitral and the tufted, each consisting of 25 pro-

jection neurons, 25 periglomerular cells and 100 granule cells (Li and Cleland, 2013). We used these two networks to investigate the mechanisms responsible for the distinct response properties between mitral and tufted cells after odor-simulating inputs. Single-cell and network parameters were systematically modified and the effect of each modifications in the network output was examined. Using this approach we were able to identify optimum parameters for the two networks that corresponded to the main differences reported in literature (Igarashi et al., 2012, Nagayama et al., 2004) in response to odor stimuli. In particular, compared to mitral cells, tufted cells responded to the simulated odor input with increased firing rates and shorter response onset latency. Finally, we conducted experiments to investigate the ability of these parallel networks to code for the concentration of the odor input and to differentiate similar input patterns. Overall, our results are in agreement with the view that the two networks use different mechanisms to encode different aspects of odor information.

2 | Literature Review

2.1 The mammalian olfactory system

2.1.1 Structural and neuronal elements of the olfactory bulb

2.1.1.1 The compartmentalized olfactory bulb

The mammalian olfactory bulb is not a uniform structure but rather a compartmentalized one. There is a left and a right olfactory bulb, each of which consists of two distinct anatomical structures, the main olfactory bulb and the accessory olfactory bulb. The accessory olfactory bulb is responsible for the detection of pheromones and other odor stimuli that are related to social and reproductive behaviors. The main olfactory bulb processes the majority of the olfactory cues. It can be further subdivided into distinct dorsal and ventral domains all of which consist of two mirror structures, a medial and a lateral. The different compartments of the main olfactory bulb have been linked to different behaviorally-relevant odorant responses. (Mori and Sakano, 2011)

The main olfactory bulb is a layered structure, with distinct neural elements in each layer. From superficial to deep these are (Mori, 2014, Shepherd et al., 2004):

1. The olfactory nerve layer (ONL)
2. The glomerular layer (GL)
3. The external plexiform layer (EPL)
4. The mitral cell layer (MCL)
5. The internal plexiform layer (IPL)

6. The granule cell layer (GCL)

2.1.1.2 Input from olfactory sensory neurons

The neuronal structures participating in the network of the olfactory bulb can be classified, like in most brain regions, into three groups. First, there are the input fibers formed by the axons of the olfactory sensory neurons. The olfactory sensory neurons are excited when an odor molecule interacts with their olfactory receptors located in the nasal epithelium. Axons from olfactory sensory neurons expressing different olfactory receptor types (~1000 different types in rodents) terminate in distinct spherical regions of the glomerular layer, namely the glomeruli. There are usually two target glomeruli for axons of olfactory sensory neurons expressing the same receptor type, the medial and lateral mirror glomeruli. These fibers transmit the odor related signals to both principle neuron and local interneurons of the olfactory bulb.(Shepherd et al., 2004)

2.1.1.3 The mitral and the tufted principal neurons

Principle neurons are the second neuronal element and can be subdivided into two main subtypes, the mitral and the tufted cells. Mitral and tufted cells, being both projection neurons, share many common features. They do, however, differ significantly in many biophysical, synaptic and functional properties.

Common morphological features Both cell types consist of a soma, an axon (with axon collaterals within and outside the olfactory bulb) and three dendritic compartments. The first compartment is the primary (basal) dendrite that originates from the soma, is located vertically in relation to olfactory bulb layers and terminates within the glomerulus. At the end of the primary dendrite originates the second dendritic compartment, the dendritic tuft. The tuft consists of many thin branches located within one glomerulus

and is the site of input from both olfactory sensory neurons and glomerular layer interneurons (Wachowiak and Shipley, 2006). Lastly, both cells give rise to several basal dendrites, referred to as secondary or lateral dendrites, located horizontally at different depths of the EPL. These dendrites are the synaptic site with another type of inhibitory interneurons, the granule cells. (Nagayama et al., 2014)

Anatomical differences Cell bodies of mitral cells are relatively large and lie mainly in the MCL. Their lateral dendrites are located mainly in the deeper half of EPL. On the other hand, cell bodies of tufted cells can be found both in the EPL and the GL. Their lateral dendrites extend mainly to the superficial half of the EPL and are less dense than those of mitral cells. (Orona et al., 1984). Both cell types have been shown to consist of distinct subpopulations (Macrides et al., 1985).

Subtypes of mitral and tufted cells Mitral cells can be further subdivided into type I and type II. Lateral dendrites of type I mitral cells are located deep in the EPL, while those of type II mitral cells are located in the intermediate part of the EPL (Orona et al., 1984, Shepherd et al., 2004). Tufted cells can be further subdivided into three subtypes according to the location of their cells bodies (Cajal, 1911, Nagayama et al., 2014, Orona et al., 1984, Shepherd et al., 2004). The three subtypes are internal, middle and external tufted cells and their soma size and dendritic field of lateral dendrites decrease from deep to superficial. Internal tufted have their cell bodies within the deep part of the EPL and they extend their lateral dendrites in the intermediate and superficial EPL. Cell bodies of middle tufted cells are located in the intermediate and superficial EPL and extend shorter lateral dendrites into the same parts of the EPL. External tufted cells are located even deeper than internal and middle tufted cells and have very short or no lateral dendrites. It is now established that part of the external tufted cell population are not projection neurons but rather local interneurons, since

they extend no axon outside the olfactory bulb.

Differences in local axon collaterals Principal neurons of the olfactory bulb extend local axon collaterals within the olfactory bulb. The distribution of these fibers, however, is far more extensive for tufted compared to mitral cells, in contrast to the distribution of their lateral dendrites. Tufted cell subtypes have been shown to extensively extend recurrent axon collaterals to the IPL (Igarashi et al., 2012). Even more, tufted cells are responsible for linking the lateral and medial mirror glomeruli (receiving input from olfactory sensory neurons expressing the same receptor type) of the olfactory bulb through their local axon collaterals (Lodovichi et al., 2003).

Differences in axon collaterals to the olfactory cortex All principal neurons of the olfactory bulb also project axon collaterals to the different areas of the olfactory cortex through the lateral olfactory tract. However, mitral cells and the different subtypes of tufted cells have different projection patterns to olfactory cortex regions (Haberly and Price, 1977). Briefly, middle and external tufted cells project only to anterior regions (anterior olfactory nucleus, olfactory tubercle and anterior piriform cortex), while mitral and internal tufted cells project to both anterior and posterior regions of the olfactory cortex (anterior olfactory nucleus, olfactory tubercle, anterior and posterior piriform cortices, amygdaloid cortex, entorhinal cortex) (Igarashi et al., 2012, Nagayama et al., 2010, 2014). Although both mitral and tufted cells project to anterior regions of the olfactory cortex areas they target distinct subregions (Igarashi et al., 2012).
The main anatomical differences between mitral and tufted cells are summarized in table 2.1.

Table 2.1: Summary of anatomical differences

	Mitral	Tufted
Cell bodies location	MCL	Subtype specific, generally deeper
Size of soma, length of primary and lateral dendrites	Large	Small, depends on somatic location (decreasing from deep to superficial)
Distribution of lateral dendrites	Mainly in the deeper half of the EPL	Mainly in the superficial part of EPL (subtype specific exact position)
Distribution of local axon collaterals within the olfactory bulb	Not extensive	Extensive recurrent collaterals in the IPL and projections to mirror mediolateral regions.
Distribution of axon collaterals to the olfactory cortex	Project to all areas of the olfactory cortex (anterior and posterior)	Internal tufted cells project to both anterior and posterior, while middle and external project only to anterior regions of the olfactory cortex.

(Igarashi et al., 2012, Shepherd et al., 2004)

Principle neurons further transmit the signals from olfactory sensory neurons to the different olfactory cortex areas, but only after their output is shaped by the activity of numerous local interneurons.

2.1.1.4 Local interneurons

Local interneurons of the olfactory bulb, the third neural element of the triad, far outnumber projection neurons unlike other regions of the central nervous system (Sakamoto et al., 2014). They constitute a highly diverse neuronal population with new subtypes still being identified (Merkle et al., 2014).

Granule cells Granule cells (GCs) are the most abundant type of interneurons in the olfactory bulb and are characterized by the lack of axons. Their cell bodies are located deeper than the cell bodies of mitral cells, in different depths. According to the depth of the soma they have been traditionally categorized into three groups: Intermediate GCs (type I) whose dendrites can be found at all depths of the EPL and can interact with both mitral and tufted cells; Deep GCs (type II) whose dendrites interact mainly with mitral cell dendrites in the deeper parts of the EPL; Superficial GCs (type III) whose dendrites interact mainly with tufted cell dendrites in the superficial EPL. Association with different subtypes of GCs is another characteristic difference between mitral and tufted cells. (Shepherd et al., 2004). GCs make reciprocal dendrodendritic synapses with the lateral dendrites of principal neurons. These synapses are characterized by glutamate mediated excitatory synapses from principal neurons to granule cells and by GABA mediated inhibitory synapses from granule cells to principal neurons (Sakamoto et al., 2014).

Periglomerular cells Another type of olfactory bulb interneurons are the glomerular layer interneurons (juxtaglomerular cells), a rather diverse group of neurons. These interneurons are located close to the glomeruli and depending on the subtype they can make connections either with neurons in one glomerulus (intraglomerular) or with neurons belonging to different glomeruli (interglomerular). One of the main subtypes of glomerular layer interneurons is the periglomelurar cell (PGC). Cell bodies of PGCs are small and located close to glomeruli, their dendritic branches arborize within glomeruli

and they can synapse with dendritic tufts of principal neurons (dendrodendritic synapses) and with axons of olfactory sensory neurons. Their axons can distribute to an area as far as six glomeruli away. PGCs can be further subdivided into type I that receive direct input from olfactory sensory neurons and type II that do not (Nagayama et al., 2014).

External tufted interneurons Other interneurons of the glomerular layer are the external tufted interneurons. These neurons can be morphologically distinguished from projecting external tufted cells since they have no secondary dendrites and they extend no axon outside the olfactory bulb. They receive direct input from olfactory sensory neurons and they are characterized by their ability to generate rhythmic bursts (Hayar et al., 2004). External tufted cells are considered to mediate an indirect excitation of mitral cells from olfactory sensory neurons (Gire et al., 2012, Najac et al., 2011).

Short axon cells Another type of olfactory bulb local interneurons is the short-axon cell. These cells consist of different subtypes. The superficial short axon cells are located in the glomerular layer and consist of at least two subtypes, one of which has dendrites contacting up to 50 glomeruli. Another subpopulation of short axon cells is located in the external plexiform layer. Finally, there are the deep short-axon cells that also consist of different subtypes. (Nagayama et al., 2014). Short axon cells and periglomerular cells can be excited by external tufted interneurons (Hayar et al., 2004).

Other subtypes Other types of olfactory bulb interneurons include Van Gehuchten cells and multipolar-type cells. The exact subtypes of interneurons, their connectivity properties and their functional roles are still not fully elucidated. For review on olfactory bulb interneurons see Nagayama et al. (2014) and Wachowiak and Shipley (2006).

Adult neurogenesis An important feature of the olfactory system is adult neurogenesis that accounts for both interneurons of the olfactory bulb and olfactory sensory neurons. Adult born PGCs and GCs originate from the subventricular zone of the lateral ventricle while adult born olfactory sensory neurons develop from basal cells located in the nasal epithilium.

2.1.1.5 Sizes of the different neuronal subpopulations

The exact numbers of each cell subtype differ between species and are not clearly established for most mammalian species. In the rabbit olfactory bulb there are approximately $50{\cdot}10^6$ olfactory sensory neurons, $2{\cdot}10^3$ glomeruli, $50{\cdot}10^3$ mitral cells and $100{\cdot}10^3$ tufted cells. Ratios of local interneurons to principal neurons have been estimated to be 20:1 periglomerular to mitral, 50-100:1 granule to mitral and 1:1 short axon to mitral (Shepherd et al., 2004).

2.1.1.6 Neuromodulatory input

Importantly, the axons of the olfactory sensory neurons are not the only input fibers into the olfactory bulb. The olfactory bulb network is further modulated by both cortical and subcortical inputs. Cortical inputs can interact with different neuronal elements of the olfactory bulb, like the granule cells, to affect the output of the olfactory bulb (Shepherd et al., 2004). Subcortical modulation of the olfactory bulb network is mediated by cholinergic, noradrenergic and serotonergic inputs.

2.1.2 Spatiotemporal coding

The olfactory bulb encodes odor-related signals both with the spatial distribution and the temporal structure of neuronal responses. The mammalian olfactory system includes ~1000 types of olfactory sensory neurons, each characterized by the expression of a specific odorant receptor in its cilia. Sensory

neurons expressing the same receptor converge to specific glomeruli. An odor molecule can activate many but specific olfactory receptors and subsequently glomeruli. What is more, a given olfactory receptor can respond to multiple odor molecules. This way the combination of the activated glomeruli forms the spatial map of the odor representation (Mori and Sakano, 2011).
To further enhance the coding abilities of the olfactory bulb, information is also encoded in the temporal patterns of the response of projection neurons. The firing rates, the latency to first spike after stimulus onset, the firing at a specific phase of an underlying oscillation and the overall pattern of spike times of projection neurons can encode different aspects of the odor stimulus. The mitral and the tufted projection neurons respond to the same stimulus with different spatiotemporal patterns. The mechanisms differentiating their responses and the functional role of this parallel processing are not fully elucidated (Uchida et al., 2014).

2.1.3 Sniff rhythm and other oscillations

Neural oscillations refer to rhythmic neural activities commonly encountered during information processing by the central nervous system networks. They can have different functional roles such as synchronizing neuronal ensembles or setting a reference point for phase preference of neuronal responses. Examples of such oscillations are the rhythm of whisking used by the somatosensory system and the theta, beta and gamma oscillations in the hippocampus that have been correlated with spatial information coding (Grossberg, 2009, Klausberger et al., 2003, Kleinfeld et al., 2016).
In the olfactory system sniff rhythm, gamma and beta oscillations set the tempo for the firing of olfactory bulb neurons (Kay et al., 2009). Sniffing rhythm in terrestrial vertebrate is generated by the synchronized processes of inhalation and exhalation. The importance of sniff rhythm in olfactory information processing is evident by the fact that it controls the timing of interaction of odor molecules with odorant receptors (Shusterman et al., 2011).

Rodents explore the environment of odorants with a rhythm ranging from 2-12 Hz with the higher frequencies occurring during active olfactory tasks (Verhagen et al., 2007). Timing of responses with regard to sniff rhythm have been shown to differ significantly between mitral and tufted cells (Fukunaga et al., 2012, Igarashi et al., 2012) and to play an important role in odor discrimination (Shusterman et al., 2011).
Gamma and beta oscillation are faster (40–90 and 15–30 Hz respectively) and nested into the sniff rhythm (Fourcaud-Trocmé et al., 2014). Generation of gamma oscillations has been associated with the reciprocal connections between principal neurons and granule cells. Gamma oscillations seem to have a prominent role in odor discrimination. Beta oscillations, on the other hand, have been linked to learning procedures of odor discrimination (Fourcaud-Trocmé et al., 2014). From different studies it has been shown that tufted cells convey odor related information to the olfactory cortex through early onset (with regard to sniff rhythm), fast gamma oscillations, whereas mitral cell with later onset, slower gamma oscillations (Mori, 2014).

2.2 Differences between mitral and tufted cells

The anatomical differences mentioned above are not the only properties differentiating mitral and tufted cells. They have also been shown to differ in intrinsic biophysical properties and in synaptic properties. Importantly, all these differences lead to distinct response properties, implying distinct functional roles for the mitral and the tufted cell populations.

2.2.1 Differences in synaptic properties

Recent studies have revealed that tufted cells are mainly excited by direct monosynaptic excitatory synaptic input from olfactory sensory neurons, whereas mitral cells mainly by indirect feedforward excitatory inputs (Gire et al., 2012, Najac et al., 2011). The pathway of the indirect inputs, the

exact synaptology and the degree of indirect versus direct excitatory inputs are not clearly established yet. It has been proposed that direct signals from olfactory sensory neurons to mitral cells exist but are being shunted due to the presence of high conductance gap junctions (Gire et al., 2012). Alternatively, the weaker direct excitation from olfactory sensory neurons reported for mitral compared to tufted cells could be due to fewer synapses.
Mitral and tufted cells also differ in their connection with local inhibitory interneurons. One well established difference is the already mentioned interaction with different subtypes of granule cells. It is also well established that the longer lateral dendrites of mitral cells allow more inhibitory inputs from granule cells and other lateral dendrite-associated interneurons (Christie et al., 2001). This also means that mitral cells are inhibited by the activity of neighboring glomeruli more strongly than tufted cells (Nagayama et al., 2004). These main synaptic differences between mitral and tufted cells are summarized in table 2.2.

Table 2.2: Summary of synaptic differences

	Mitral	Tufted
Excitatory input from olfactory sensory neurons[1,2]	Mainly indirect, weak monosynaptic	Mainly direct, strong monosynaptic
Granule cell subtype[3]	Type II (deep)	Type III (superficial)
Inhibitory input at the lateral dendrites[4]	Extensive	Limited

[1](Gire et al., 2012), [2](Burton and Urban, 2014), [3](Shepherd et al., 2004), [4](Christie et al., 2001)

2.2.2 Differences in electrophysiological properties

Although anatomical differences between mitral and tufted cells have been known for decades (Cajal, 1911), detailed examination of differences with re-

gard to electrophysiological properties was lacking until recently (Burton and Urban, 2014). Burton and Urban (2014) showed that mitral cells have higher membrane capacitance and slightly lower input resistance than tufted cells, correlated with the larger size of mitral cells. They also showed that tufted cells fire action potentials of shorter duration and with faster afterhyperpolarization compared to mitral cells. Moreover, when compared to mitral cells, tufted cells exhibited two times greater peak firing rates and increased firing rates after somatic step current injections of incrementing amplitude. Also, the two cell types exhibited differences in the firing modes after somatic current injections: tufted cell firing was on average more irregular than mitral cell firing. All these differences most probably arise from different intrinsic biophysical properties between mitral and tufted cells, including their morphological differences and differences in membrane properties such as ionic channel conductances. The exact correlations, however, are not clear yet. Differences in electrophysiological properties are summarized in the next table.

Table 2.3: Summary of electrophysiological differences

	Mitral	Tufted
Membrane capacitance	High	Low
Input resistance	Low	High
Action potential duration	Long	Short
Duration of afterhyperpolarization	Long	Short
Overall intrinsic excitability	Low	High
Firing rates after somatic current injections	Low	High
Firing mode	More regular	More irregular

[1](Burton and Urban, 2014)

2.2.3 Differences in the response after odor-evoked stimulation

The synaptic and intrinsic biophysical differences between mitral and tufted cells are highly likely to give rise to different firing properties in response to the same odor input. Numerous recent studies have revealed such differences in the odor-evoked response properties of the principal neurons. We summarize these differences in the following table.

Table 2.4: Summary of differences in odor-evoked response properties

	Mitral	Tufted
Odor-evoked firing rates [1,2]	Lower	2-3 times higher
Latency of response onset [3,4]	Longer	Shorter
Change of response latency with decreasing concentration	Increase[3]	Increase[3] or no change[4]
Odor concentration threshold[3,5]	Higher	Lower
Excitatory receptive range*[,5]	Finer	Wider
Inhibitory receptive range**[,1]	Robust	Weak
Response to mixtures***[,1]	Decreased	Unaffected

[1](Nagayama et al., 2004), [2](Griff et al., 2008), [3](Igarashi et al., 2012), [4](Fukunaga et al., 2012), [5](Kikuta et al., 2013)
*Spectrum of odor molecules that can activate a neuron.
**Spectrum of odor molecules that can inhibit a neuron.
***Change of the response of a neuron to a given odorant after adding odorants that activate other glomeruli.

Mechanisms generating these differences are not known and are one of the aims of this study.

2.2.4 Experimental data on the distinct properties of mitral and tufted cells

One of the most important parts in the process of modeling a biological system is the data used for the model's validation. It is not unusual that these data are not coherent across literature. In studies of the olfactory system such incoherencies can be due to a number of parameters, including different experimental conditions (in vitro, in vivo in anesthetized animals using different anesthetics, in vivo in awake animals), experiments on different animal species, different measurement techniques (electrophysiology, calcium imaging), stimulation with different odor molecules, different methods of identifying subtypes of neurons and even differences in data analysis.

2.2.4.1 Data on differences in response latency

In 2012 two in vivo studies were published comparing the timing of the response between mitral and tufted cells.
In the first sudy (Igarashi et al., 2012) it is shown that tufted cells respond faster to odor stimuli. Tufted cells showed reliable responses 108±12 ms (mean ± standard deviation) after onset of inhalation, while mitral cells after 252±12 ms. Timing of response was calculated using a reliability index that compared the stimulus response to the spontaneous firing rate. This study was conducted in anesthetized mice. Labeling of a neuron as mitral or tufted was done based on soma location: cells with soma location in the MCL were labeled as mitral and cells with soma location in EPL as tufted (tufted cells were further classified as external, middle or internal).
In the second study (Fukunaga et al., 2012) it was shown that mitral and tufted cells preferentially fire in different phases of sniff rhythm. Tufted cells preferentially fire at 240.3 ± 43.2 ms, while mitral cells at 475.5 ± 91.1 ms after odor inhalation. Experiments were conducted on anesthetized OR174 transgenic mice. Sorting of principal neurons was done by identifying two

clusters of principal neurons based on soma location and size and dendritic location and length, that corresponded to mitral and tufted cells.
In 2014 an in vitro electrophysiological study compared both the intrinsic biophysical properties and the response properties of mitral and tufted cells to afferent-evoked stimulation (Burton and Urban, 2014). In this study the response latency of tufted cells was found to be ~25-50 ms (depending on stimulation frequency and cycle of stimulation) shorter than that of mitral cells. The study was conducted in mice olfactory bulb slice preparations. Principal neurons were initially identified by their large cell bodies and their primary dendrite. Next, they were labeled as mitral if more than 50% of their cell body was located in the MCL, and as tufted if theirs cell bodies were located completely within the EPL.

2.2.4.2 Data on differences in odor-evoked firing rate

The study of (Nagayama et al., 2004) reports experimental data on the different firing rates between mitral and tufted cells. Specifically, the spontaneous and odor-evoked firing rates for mitral cells were found to be 7.4 ± 6.6 (mean ± standard deviation) and 41.5 ± 13.1 respectively. The corresponding values for tufted cells were 16.9 ± 21.1 and 103.0 ± 63.8. Experiments were conducted in anesthetized rats. In this study neurons were labeled as mitral if they were located in the MCL and as tufted if they were located in the EPL. Researchers compared the properties of mitral and tufted cells belonging to anatomically clustered glomeruli.
In the in vitro study of Burton and Urban (2014) tufted cells also exhibited higher (2-4 times) firing rates compared to mitral cells in response to afferent-evoked excitation.

3 | Methodology

3.1 Harware and Software

All single cell and network simulations were implemented in the NEURON simulator package, version 7.3 (Carnevale and Hines, 2006). Simulations exploring multiple parameters were processed by a cluster consisting of 312 High Performance CPU cores and 1.150 Gigabytes of RAM, running Red Hat -Centos Linux (version 6.5) and administered by the Computational Biology Lab (CBL) of the Institute of Molecular Biology and Biotechnology (IMBB) of the Foundation for Research and Technology Hellas (FORTH). Single testing trials were run on a dedicated 28-core, 128 GB RAM Linux Server. Data analysis was conducted with MATLAB (Mathworks Inc.).

3.2 Adopted model of a mitral cell

We defined as "initial model" the morphological, biophysical and network parameters of the study of Li and Cleland (2013). This model was used as a starting point for our simulations and was subject to modifications to replicate experimental data (see section 4.1).
The "initial cell model" is a morphologically simplified compartmental biophysical model of a mitral cell implemented in NEURON simulation environment (Li and Cleland, 2013). The model consists of 4 compartments: the soma, the lateral dendrite, the primary dendrite and the tuft dendrite. Morphological characteristics of each compartment are presented in table 3.1. Other properties of the model are presented in table 3.2.

	Soma	Lateral	Primary	Tuft
Length (μm)	25	370	500	20
Diameter (μm)	20	3.5	3.4	0.5

Table 3.1: Morphological properties for each compartment of the "initial cell model", (soma, lateral dendrite, primary dendrite and dendritic tuft).

Membrane resistance (Rm)	$30{\cdot}10^3$ $\Omega{\cdot}cm^2$
Na equilibrium potential (E_{Na})	45 mV
K equilibrium potential (E_K)	-80 mV
Axial resistance (Ra)	70 $\Omega{\cdot}cm$
Specific membrane capacitance (cm)	1.2 $\mu F/cm^2$

Table 3.2: Biophysical properties of the "initial cell model".

The model also includes the following ionic channels:

* Passive channels: Equilibrium potential=-60 mV, conductance=1/Rm.
* Sodium channels: Transient sodium channel (Na_f) and persistent sodium channel (Na_p).
* Potassium channels: Delayed rectifier (K_{DR}), slow-inactivating (K_s), Ca^{2+} activated(K_{Ca}) and transient potassium channel (K_A).
* Calcium channels: High threshold L-type Ca^{2+} (LCa)

Conductances of the active channels in each compartment are presented in table 3.3.

	Soma	Lateral	Primary	Tuft
Na_f	50	30	20	20
Na_p	0.2	0.02	0.10	0.10
K_{DR}	30	20	10	10
K_s	42	8	18	18
K_A	10	0	0	0
K_{Ca}	5	0	0	0
LCa	0.4	0.05	0.2	0.2

Table 3.3: Channel conductances of the "initial cell model". Units in 10^{-3} S/cm^2

.

For more details, this model is available for download in ModelDB with accession number: 149739.

3.3 Single cell simulations

3.3.1 Simulation protocols

For the electrophysiological measurements we stimulated the single cells with somatic current injections, delivered 2 seconds after the initiation of the simulation and for a duration of 2 seconds. Cells were simulated with -300, -250, -200, -150, -100, -50, 10, 20, 30, 40, 50, 60, 70, 80, 90, 100, 110, 120, 130, 140, 150, 160, 170, 180, 190, 200, 210, 220, 230, 240, 250, 260, 270, 280, 290 and 300 pA at independent trials. The total recording time was 5 seconds.

3.3.2 Electrophysiological measurements

In this section we present the electrophysiological properties used to validate the single cell models. Measurements were done according to the methods reported at the experimental study of Burton and Urban (2014) to enable comparison.

Passive properties

* Resting membrane potential (V_{rest}): determined as the voltage 100ms before current injection.

* Input resistance (R_{in}): calculated by the formula $R_{in} = \frac{\Delta V}{\Delta I_e}$.

  ΔV (change in membrane potential) is calculated during -100 pA somatic current injection by subtracting the voltage value 100 ms before the end of the current injection (steady state, at 3900 ms) from the voltage value 200 ms before the current injection (resting state, at 1800 ms). ΔI_e is the change in the injection current (0.1 nA).

* Membrane time constant (τm): measured during -100 pA somatic current injection and corresponding to the time required for the voltage to reach 63% of its final value.

* Membrane capacitance (Cm): calculated by the formula $Cm = cm \cdot Area_{total}$. $Area_{total}$ is the sum of the areas of each compartment that are calculated by the formula $Area = 2 \cdot \pi \cdot diameter \cdot length$.

* Sag amplitude: measured at the negative current input trial that resulted in steady state voltage closest to -90mV, calculated as the minimum voltage reached the first 300 ms after the current injection subtracted from the steady state voltage.

Action potential properties

These properties were calculated from the first action potential at rheobase input. The onset of an action potential was determined as the time at which the derivative of the voltage exceeded 20 mV ms^{-1}.

* $V_{threshold}$: Voltage at the onset of the action potential.
* Action potential amplitude: measured by subtracting the voltage at the onset of the action potential from the peak voltage.
* Full action potential width at half-maximal amplitude (FWHM): the width (in ms) of the action potential at the half of its amplitude.
* AHP amplitude: calculated as the first local minimum after the onset of the action potential subtracted from $V_{threshold}$.
* Duration of AHP (τAHP 50%): calculated as the time from AHP start to the time that the voltage returned to 50% of AHP amplitude. The start of AHP was determined as the time after the action potential that the voltage reached $V_{threshold}$.

Spike train properties

* Rheobase: defined as the weakest input generating an action potential.
* Rheobase first spike latency (RSL): calculated as the time of the first spike at rheobase input.
* First spike latency after 100 pA somatic current injection (SL_{100pA}): calculated as the time of the first spike at 100 pA somatic current injection.
* FI curve gain: calculated as the maximum firing rate gain between two successive step current injections.

* Firing rate at 300 pA current input ($FR_{300\ pA}$): the mean firing rate during the 2 second-long 300 pA current injection.

3.4 Network simulations

3.4.1 Network description

The cell models obtained after the validation procedure were incorporated in the "initial network" (Li and Cleland, 2013) that demonstrates the essential features of the olfactory bulb network. Specifically, this network consists of 25 projection neurons, 25 periglomerular cells and 100 granule cells. Simulated odor input is delivered at the projection neurons and at perigromerular cells. Each periglomerular cell is reciprocally connected with a projection cell at the level of the tuft and these two represent an individual glomerulus. Projection cells and granule cells are also reciprocally connected, through synapses located at the lateral dendrite of the projection neuron. Each granule cell has a 0.3 probability to connect with each one of the 25 projection neurons. Both reciprocal connections consist of an excitatory NMDA and AMPA mediated synapse from mitral/tufted cells to periglomerular/granule cells and of an inhibitory $GABA_A$ mediated synapse from periglomerular/-granule cell to mitral/tufted cells. A cartoon of the model is presented in figure 4.1.
This network is also available for download from ModelDB with the same accession number.

3.4.2 Simulated odor input

The odor input of the "initial network" was simulated as current injection delivered to the tuft of mitral cells and to periglomerular cells, representing the synaptic input from many olfactory sensory neurons. The value of the

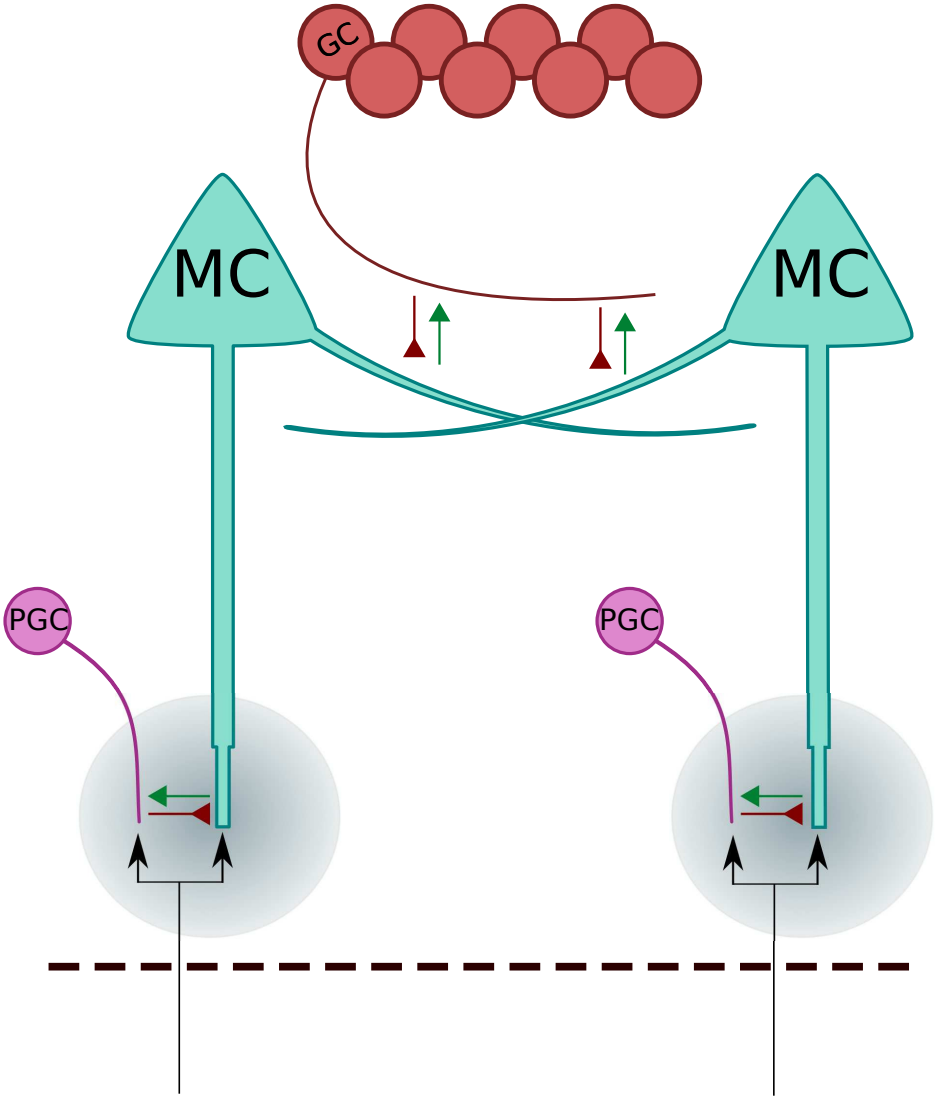

MC: mitral cell, GC: granule cell, PGC: periglomerular cell, red arrows: inhibitory synapses, green arrows: excitatory synapses, black arrows: afferent inputs, grey circles: glomeruli.

Figure 3.1: Schematic representation of the "initial network".

current injected at each time point was given by the following function:

$$I(t) = u_0 + 0.5(u_s - u_0)\left[\tanh\left(\frac{3(t - t_{ORN})}{r} - 3\right) + 1\right]$$

Current is measured in nA, u_0 (0.1-0.2 nA) is a constant preodor value simulating pure air input, u_s (nA) is the maximum odor input (different value for each glomerulus), r is a constant that determines the increase rate from u_0 to u_s and t_{ORN} is the time of odor input.
In the "initial model" (Li and Cleland, 2013) the odor input was delivered at 2s with maximum amplitude (u_s) until the end of the simulation (3s total duration). The constant r was determined at 100 s.
In our simulations we modified the function so that the odor was delivered at 2s, for 1s duration, with 2Hz frequency (to simulate two sniffs). The modified function is:

$$I(t) = u_0 + 0.5(u_s - u_0)\Bigg[\tanh\left(\frac{3(t - t_{start1})}{r_1} - 3\right) - \tanh\left(\frac{3(t - t_{stop1})}{r_2} - 3\right) + \tanh\left(\frac{3(t - t_{start2})}{r_1} - 3\right) - \tanh\left(\frac{3(t - t_{stop2})}{r_2} - 3\right)\Bigg]$$

t_{start1}, t_{start2}, t_{stop1} and t_{stop2} were set at 2000, 2500, 2200 and 2700 respectively. The constants r_1 and r_2 were set at 50 and 150 s respectively. For all network simulations we recorded for a total time of 10 s.
The initial and the modified current amplitude plotted against time and for u_0=0.2 and u_s=1 are presented in figure 3.2.

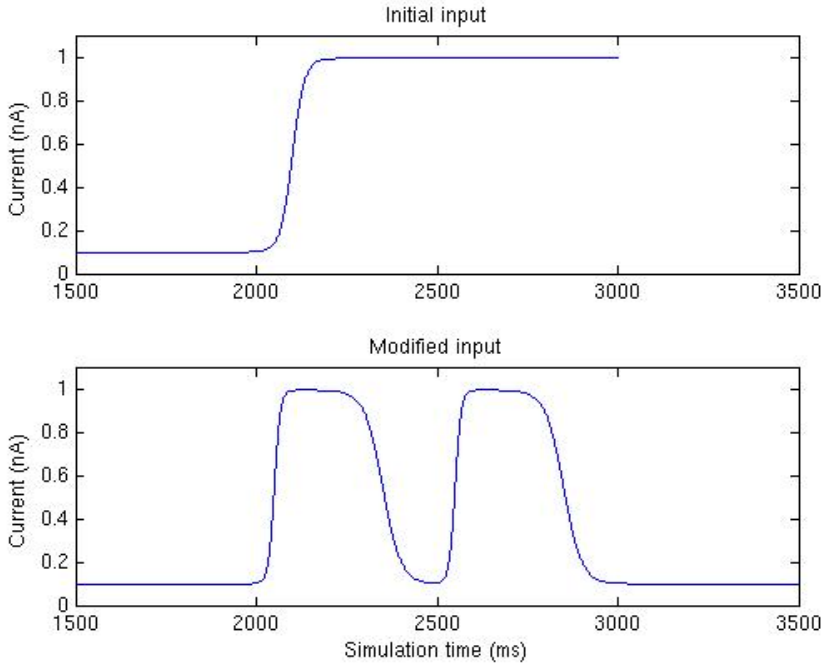

Figure 3.2: Time course of odor input during network simulations.

For all network experiments the preodor input (u_0) for each one of the 25 projection neurons was obtained from a uniform distribution from 0.1 to 0.2 nA as in (Li and Cleland, 2013).

Each one of the projection neurons and the corresponding periglomerular cells represent a different glomerulus receiving inputs from different types of olfactory receptors that have different affinities for the same odor molecule. Therefore, each projection neuron of the network received different maximum input current (different u_s). Periglomerular cells received the same current input as their corresponding principal neuron, scaled down by 0.4.

For the network parameter exploration simulations the odor input to each one of the 25 cells was obtained from a uniform distribution from 0.2 to 1 as in the "initial model". For the simulations on the coding properties of the two networks (section 4.3) regarding different concentrations and similar

odors, the input pattern across glomeruli was modified to be more easily manipulated. Specifically, the input to each cell was determined by a normal distribution where the 13^{th} cell was the mean, receiving maximum input, and standard deviation was set to 3. This way, a different odor was assumed to have the same distribution with a different mean. Increasing-decreasing concentration was modelled by multiplying the initial input of each cell by a scalar factor, as previously suggested (Davison et al., 2003).
Preodor input, odor input for the parameter exploration experiments and odor input for the part C experiments delivered to each of the 25 principal neurons are shown in figure 3.3.

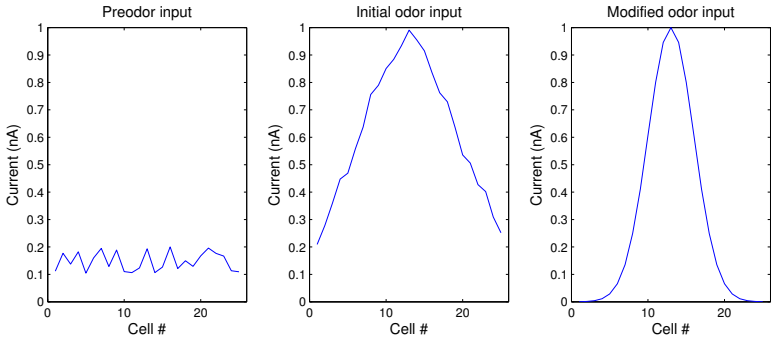

Figure 3.3: Current input for each one of the 25 projection cells.

3.4.3 Network output measurements

For the parameter exploration simulations, during network implementation we focused on the properties of the 13^{th} cell since this cell represents the glomerulus with the highest affinity for the simulated odor. However, we also present results as the mean of the coding cells (CC). The coding cells are defined as those that exhibit a statistically significant increase in their firing rate after odor input compared to their spontaneous firing rate. The statistical significance was evaluated with a Mann-Whitney U test and the p-value should be less than 0.01. Also, only cells at positions 11 - 15, receiving higher current amplitude compared to the rest of the cells, were included to

have a more coherent population. Each simulation with a given set of parameters was repeated 30 times. Results are presented as the mean plus/minus standard deviation of the 30 trials.
The main properties that we examined are:

* The spontaneous firing rate (FR_{sp}) calculated as the number of spikes during the 1 second period preceding odor input.
* The mean odor-evoked firing rate (FR_{ev}) calculated as the number of spikes during the 1 second period of odor input.
* The time-to-first spike (TTFS) after odor input in ms.

4 | Results

In this chapter we present the results of the computational simulations. At first we used recent experimental data to develop two distinct morphologically-simplified biophysical compartmental single cell models, one validated against mitral cell and the other against tufted cell electrophysiological data. Next, we incorporated these models in a representative network of the olfactory bulb. Finally, we used these two independent networks to study the mechanisms used by mitral and tufted cells to encode different odor properties.

4.1 Part A: Development of two distinct biophysical models representative of mitral and tufted cells.

We initiated our study by systematically modifying biophysical parameters of the "initial cell model" (Li and Cleland, 2013), to approximate values reported in literature.
With this approach we managed to create two representative model cells, one for the mitral and one for the tufted cell subpopulation. The modified parameters were ionic equilibrium potentials, membrane resistance, morphological properties, channel kinetic properties and channel conductances.
In order to achieve the reported values for sag amplitude we incorporated hyperpolarization-activated channels (I_h channels) in both models. Modelling equation of the channel conductance was adapted from the respective one used for the periglomerular cells of the "initial network" (Li and Cleland, 2013). Conductances for the I_h channels for each compartment are shown in table 4.1.

	Soma	Lateral	Primary	Tuft
Mitral	0.03	0.3	0.3	0.3
Tufted	0.06	0.6	0.6	0.6

Units in $9{\cdot}10^{-6}$ S/cm^2.

Table 4.1: Conductances of the hyperpolarization activated channels.

For both cells the K^+ equilibrium potential (E_K) was set to -70 to better approximate AHP values. Membrane resistance (Rm) was multiplied by 0.6 for tufted cells to adjust for the smaller morphology and the higher input resistance compared to mitral cells. Given the simplified morphology of the model, the morphological differences were approximated by uniformly multiplying the diameter and length of each compartment by a morphology factor. This factor was set to 1.2 and 0.95 for mitral and tufted cells respectively. To increase excitability for both cells, in order to approximate the reported values, we also modified channel kinetic properties. For both models the activation time constant of Na_f was multiplied by 0.1, the inactivation time constant of Na_f by 3, the activation time constant of K_s by 0.5 and the activation time constant of K_{DR} by 0.5.
The channel conductances were adjusted by uniformly multiplying the conductances of each compartment by the factors shown in table 4.2. Initial conductance values are shown in table 3.3.

	Na_f	Na_p	K_{DR}	K_s	K_A	K_{Ca}	LCa
Mitral	1.2	0.14	0.2	0.12	8	5	1
Tufted	1.2	1.1	1.2	1	8	1	0.1

Table 4.2: Multiplying factors for channel conductances for the mitral and the tufted model.

.

In table 4.3 we present the resulting biophysical properties in comparison to

the experimental data and the values of the "initial cell model".

Table 4.3: Comparison of electrophysiological properties.

	Experimental values*		Model values		
	Mitral	Tufted	Initial**	Mitral	Tufted
Passive properties					
Vrest (mV)	-53.9 ± 4.0	-55.5 ± 4.7	-68.83	-59.06	-59.00
Rinput (MΩ)	94.3 ± 40.5	111.8 ± 51.6	174.9	74.62	125.52
τm (ms)	21.3 ± 9.4	18.8 ± 8.6	26.3	14.4	13
Cm (pF)	236.4 ± 94.6	188.8 ± 110.1	150.37	190.18	119.19
Sag amplitude (mV)	2 ± 2.6	4.4 ± 6.1	0.18	2.07	3.87
AP properties					
Vthreshold (mV)	-42.2 ± 3	-42.8 ± 2.9	-36.61	-39.68	-40.05
Amplitude (mV)	76.2 ± 5.4	72.1 ± 5.5	63.13	74.77	74.35
FWHM (ms)	1.06 ± 0.2	0.87 ± 0.1	0.47	1.0714	0.84
AHP (mV)	14.8 ± 3.2	16.8 ± 3.3	39.67	28.09	29.49
τAHP 50% (ms)	58.2 ± 77.5	20.5 ± 20.1	n/a***	100.06	38.64
Sp. train properties					
Rheobase (pA)	111.4 ± 55.7	94.6 ± 49.7	120	90	20
RSL (ms)	510 ± 486	402.3 ± 479.5	1982	774.9	1216.4
SL_{100pA}			n/a***	388.3	293.1
FI curve gain (Hz)	9.8 ± 3.8	20.3 ± 7.2	3	7.5	12.5
$FR_{300\ pA}$ (Hz)	35	50	9	24.5	43.5

*Mean values and standard deviation from 10-35 cells (Burton and Urban, 2014).
**(Li and Cleland, 2013)
***n/a: not applicable

In the next figure we present the voltage traces for the two models after step current injection of increasing current amplitude. The corresponding traces

from Burton and Urban (2014) are also shown for comparison.

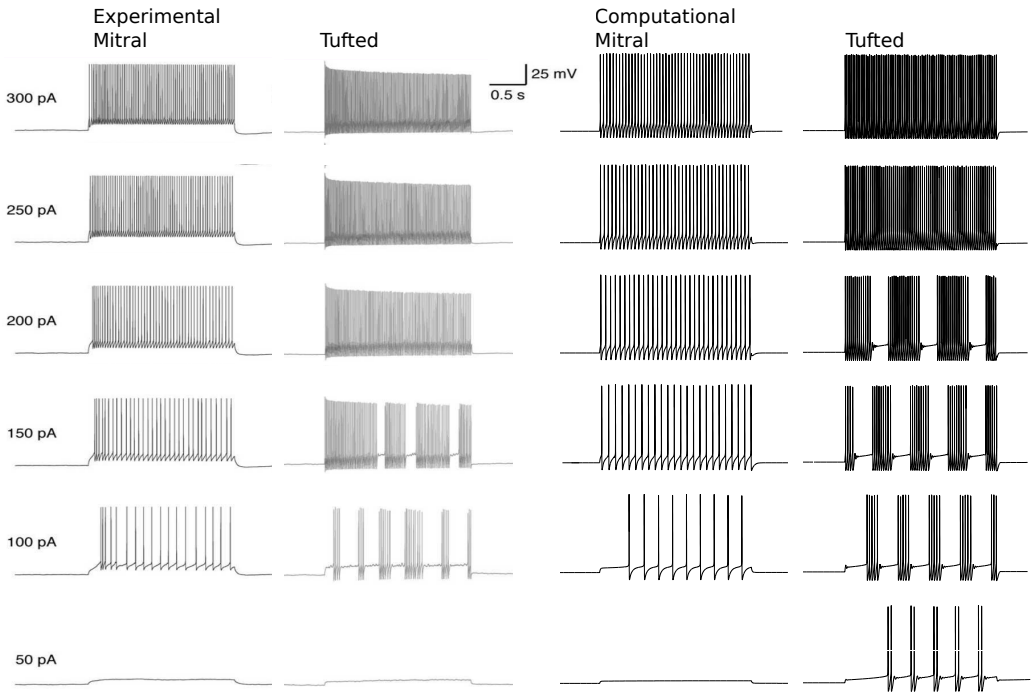

Figure 4.1: Response of mitral vs tufted cells to somatic step current injections. Experimental traces from Burton and Urban (2014)

4.2 Part B: Investigation of possible biophysical and network mechanisms responsible for differences in response properties of principal neurons

In the second part of our study we incorporated the two distinct single cell models into two independent networks, the mitral and the tufted network. Initially, the only difference between the two networks was the different biophysical models of the principal neurons. To evaluate possible mechanism of

the reported differences in the response properties, we systematically modified biophysical parameters of the principal neurons or parameters of the network. We focused on the effect of each modification on the mean odor-evoked firing rate (FR_{ev}) and the time to first spike after odor input (TTFS), since these two are well established properties differentiating the two subpopulations.
All systematic modifications were initially examined on the mitral network. With the insight gained by this approach we re-examined the most promising parameters in both networks and we ended up with two independent networks with different properties, resembling those reported by experimental studies.

4.2.1 The effect of modifying biophysical properties

In this section we present the effect of systematically modifying biophysical properties of the single cells in the FR_{ev} and the TTFS. Note that from the literature tufted cells are expected to have shorter TTFS and higher FR_{ev}. We present the values of the 13^{th} cell (center of the input distribution) as a mean of 30 trials. We also present the mean of the coding cells (see section 3.4.3 for definition) for the 30 trials.
The following figures show the effect of systematically modifying the conductance of Na_f, Na_p, K_s and K_A in the primary dendrite, the dendritic tuft or the lateral dendrite. We chose to investigate the effect of these channels only, since these channels had the most prominent effect in the timing of the first spike after 100 pA somatic current injection during the single cell validation procedure (data not shown).
X axis represents the multiplying factor for the channel conductance in each compartment and y axis represents the FR_{ev} or the TTFS. Results for both the 13^{th} cell and the mean of the coding cells are presented. For comparison reasons, the dashed line represents the corresponding values of the tufted network, without any modifications. Errorbars and width of gray area represent the standard error of the mean of the 30 trials.

Figure 4.2: The effect of modifying channel conductances of the primary dendrite in the response properties of 13th cell.

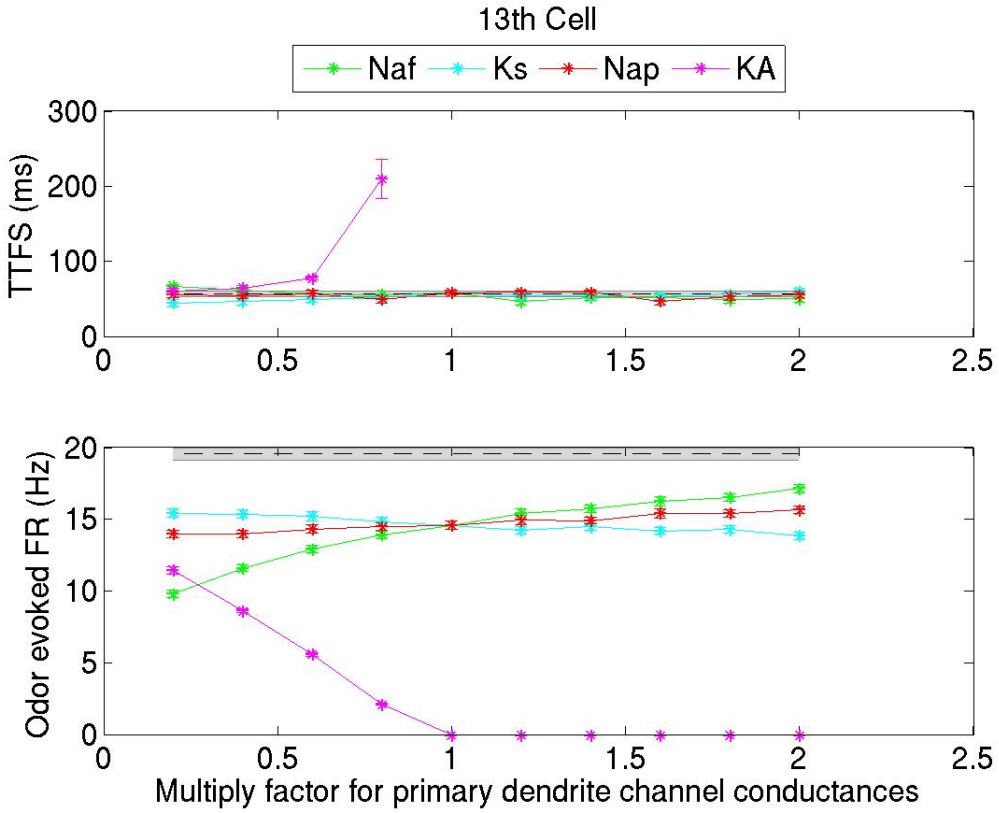

Response properties of the 13th cell. Top: Time-to-first spike (TTFS); Bottom: Odor-evoked firing rate (FR); X-axis: The scaling factors used to modify channel conductances in the primary dendrite; Naf: transient sodium channel; Nap: Persistent sodium channel; Ks: Slow-inactivating potassium channel; KA: Transient potassium channel; Dashed lines: corresponding values of the tufted network; Asterisks: mean values from 30 trials. Errorbars and width of the gray area: standard error of the mean from 30 trials.

Figure 4.3: The effect of modifying channel conductances of the primary dendrite in the response properties of coding cells.

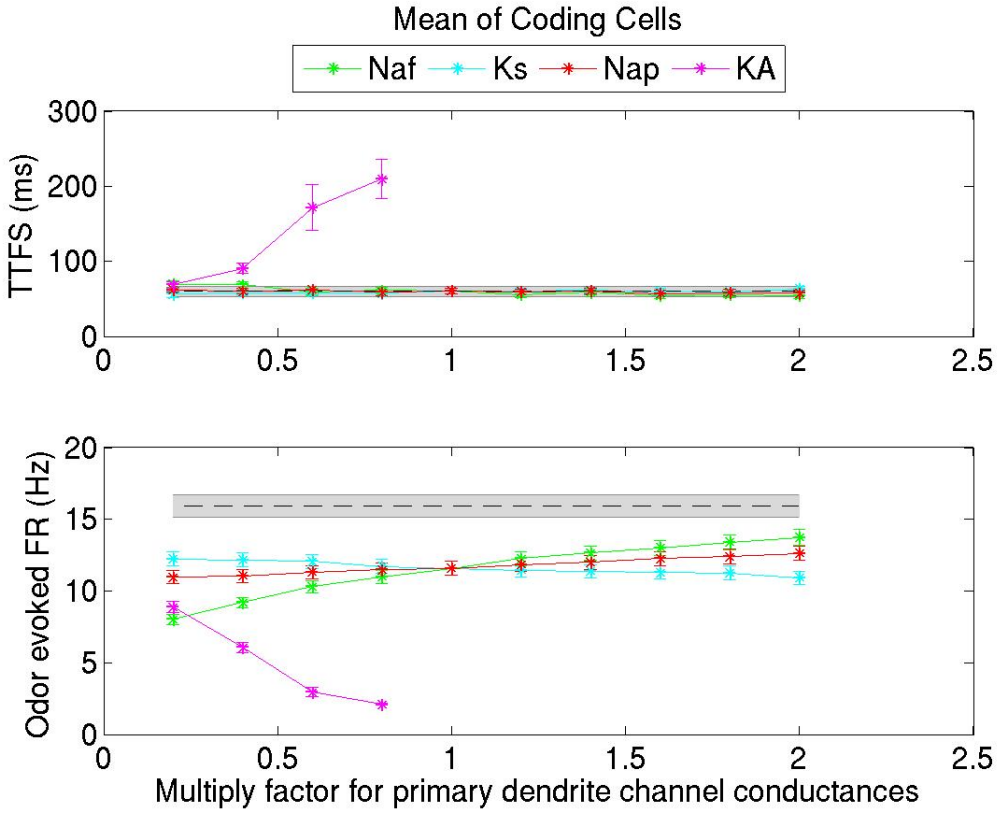

Response properties of coding cells. Top: Time-to-first spike (TTFS); Bottom: Odor-evoked firing rate (FR); X-axis: The scaling factors used to modify channel conductances in the primary dendrite; Naf: transient sodium channel; Nap: Persistent sodium channel; Ks: Slow-inactivating potassium channel; KA: Transient potassium channel; Dashed lines: corresponding values of the tufted network; Asterisks: mean values from 30 trials. Errorbars and width of the gray area: standard error of the mean from 30 trials.

Figure 4.4: The effect of modifying channel conductances of the dendritic tuft in the response properties of 13th cell.

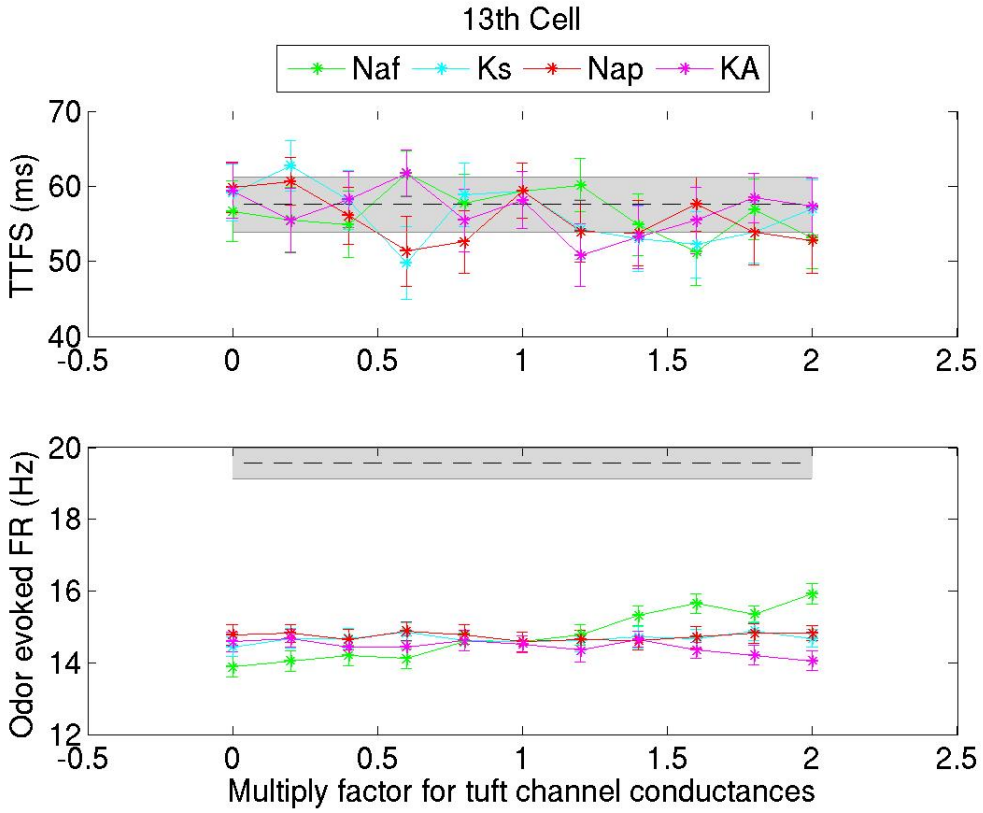

Response properties of the 13th cell. Top: Time-to-first spike (TTFS); Bottom: Odor-evoked firing rate (FR); X-axis: The scaling factors used to modify channel conductances in the dendritic tuft; Naf: transient sodium channel; Nap: Persistent sodium channel; Ks: Slow-inactivating potassium channel; KA: Transient potassium channel; Dashed lines: corresponding values of the tufted network; Asterisks: mean values from 30 trials. Errorbars and width of the gray area: standard error of the mean from 30 trials.

Figure 4.5: The effect of modifying channel conductances of the dendritic tuft in the response properties of coding cells.

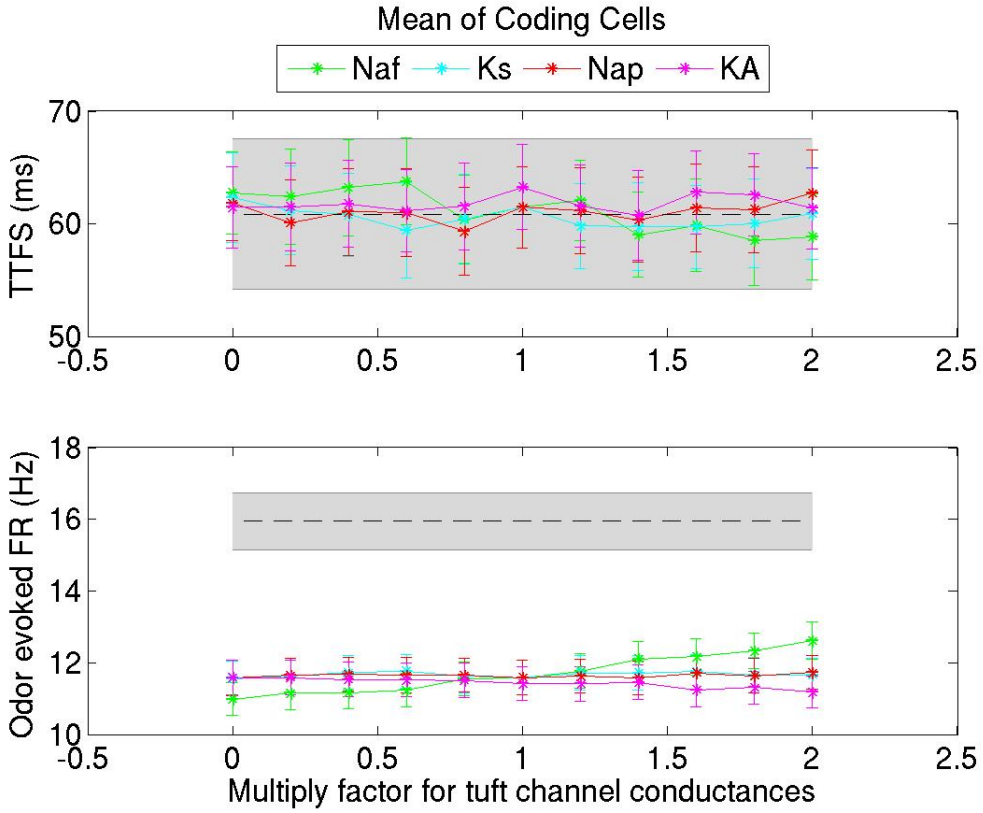

Response properties of coding cells. Top: Time-to-first spike (TTFS); Bottom: Odor-evoked firing rate (FR); X-axis: The scaling factors used to modify channel conductances in the dendritic tuft; Naf: transient sodium channel; Nap: Persistent sodium channel; Ks: Slow-inactivating potassium channel; KA: Transient potassium channel; Dashed lines: corresponding values of the tufted network; Asterisks: mean values from 30 trials. Errorbars and width of the gray area: standard error of the mean from 30 trials.

Figure 4.6: The effect of modifying channel conductances of the lateral dendrite in the response properties of 13th cell.

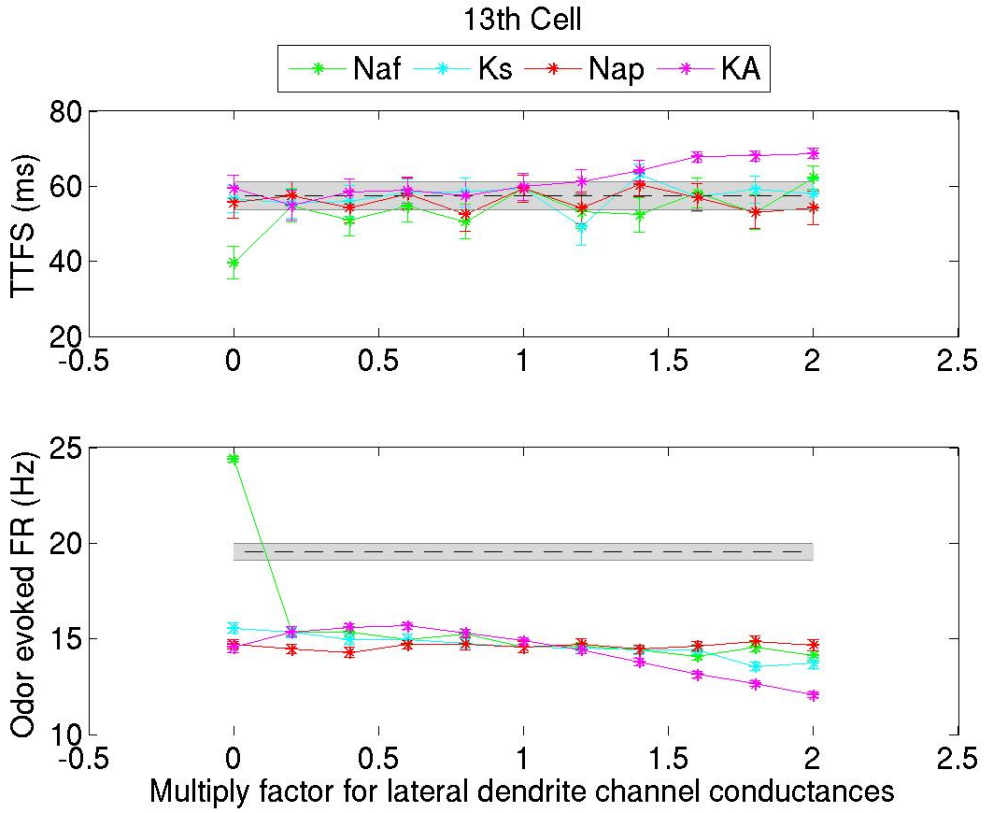

Response properties of the 13th cell. Top: Time-to-first spike (TTFS); Bottom: Odor-evoked firing rate (FR); X-axis: The scaling factors used to modify channel conductances in the primary dendrite; Naf: transient sodium channel; Nap: Persistent sodium channel; Ks: Slow-inactivating potassium channel; KA: Transient potassium channel; Dashed lines: corresponding values of the tufted network; Asterisks: mean values from 30 trials. Errorbars and width of the gray area: standard error of the mean from 30 trials.

Figure 4.7: The effect of modifying channel conductances of the lateral dendrite in the response properties of coding cells.

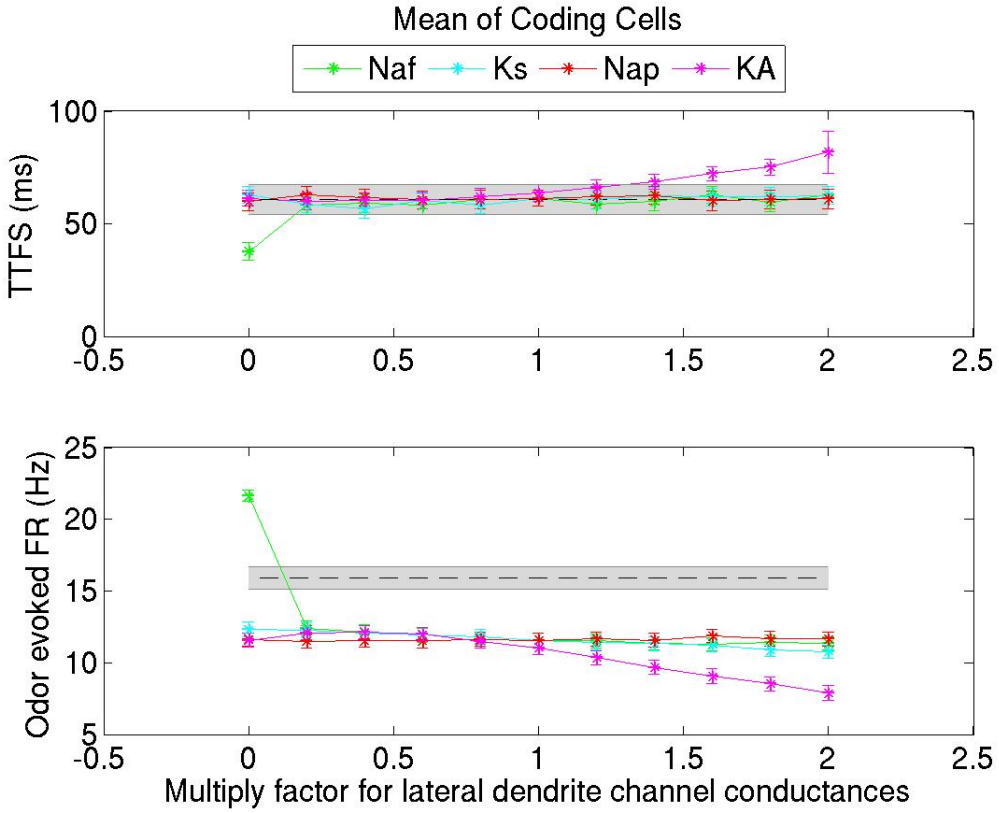

Response properties of coding cells. Top: Time-to-first spike (TTFS); Bottom: Odor-evoked firing rate (FR); X-axis: The scaling factors used to modify channel conductances in the primary dendrite; Naf: transient sodium channel; Nap: Persistent sodium channel; Ks: Slow-inactivating potassium channel; KA: Transient potassium channel; Dashed lines: corresponding values of the tufted network; Asterisks: mean values from 30 trials. Errorbars and width of the gray area: standard error of the mean from 30 trials.

For all these modifications we also evaluated their effect in single cell electrophysiological properties (data not shown). Overall, modifying channel conductances in the primary dendrite had the highest effect in modulating the response of mitral cells. Modifying parameters in the lateral dendrite and the dendritic tuft had, in general, a smaller effect. Adding K_A channels in the primary dendrite was sufficient to delay TTFS for hundreds of mil-

liseconds. However, it also depressed the FR_{ev} and decreased R_{in} and τm at levels outside the biological range. On the other hand, modifications in the conductance of Na_f channels caused a smaller shift in TTFS and FR_{ev} and did not affect the passive electrophysiological properties.

4.2.2 The effect of modifying network properties

In this section we present the results of systematically modifying network parameters. The parameters that were examined are the weight of connection from mitral cells to granule cells, from mitral cells to periglomerular cells, from granule cells to mitral cells and from periglomerular cells to mitral cells. We also examined the effect of modifying the number of granule cells, the probability of connection between mitral and granule cells and the efficacy of the synaptic input representing the input from olfactory sensory neurons to mitral cells or periglomerular cells. Modifying the efficacy of the input from olfactory sensory neurons was modelled by multiplying the current amplitude by an "efficacy" factor. As before, figures show FR_{ev} and TTFS for the 13^{th} cell and for the coding cells in relationship to modifying these parameters.

Figure 4.8: The effect in the response of the 13th cell while modifying the weight of the connection from mitral to periglomerular, from periglomerular to mitral, from mitral to granule and from granule to mitral cells.

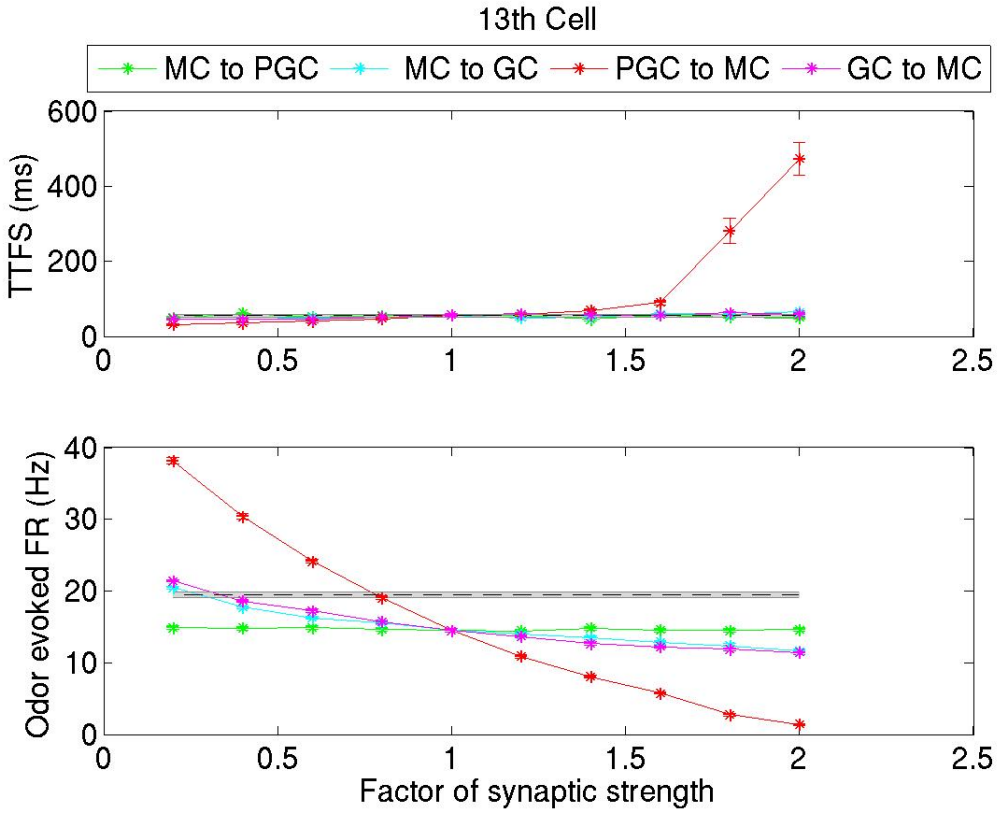

Response properties of the 13th cell. Top: Time-to-first spike (TTFS); Bottom: Odor-evoked firing rate (FR); X-axis: The scaling factors used to modify the synaptic strength; MC: mitral cell; PGC: periglomerular cell; GC: granule cell; Dashed lines: corresponding values of the tufted network; Asterisks: mean values from 30 trials. Errorbars and width of the gray area: standard error of the mean from 30 trials.

Figure 4.9: The effect in the response of coding cells while modifying the weight of the connection mitral to periglomerular, from periglomerular to mitral, from mitral to granule and from granule to mitral cells.

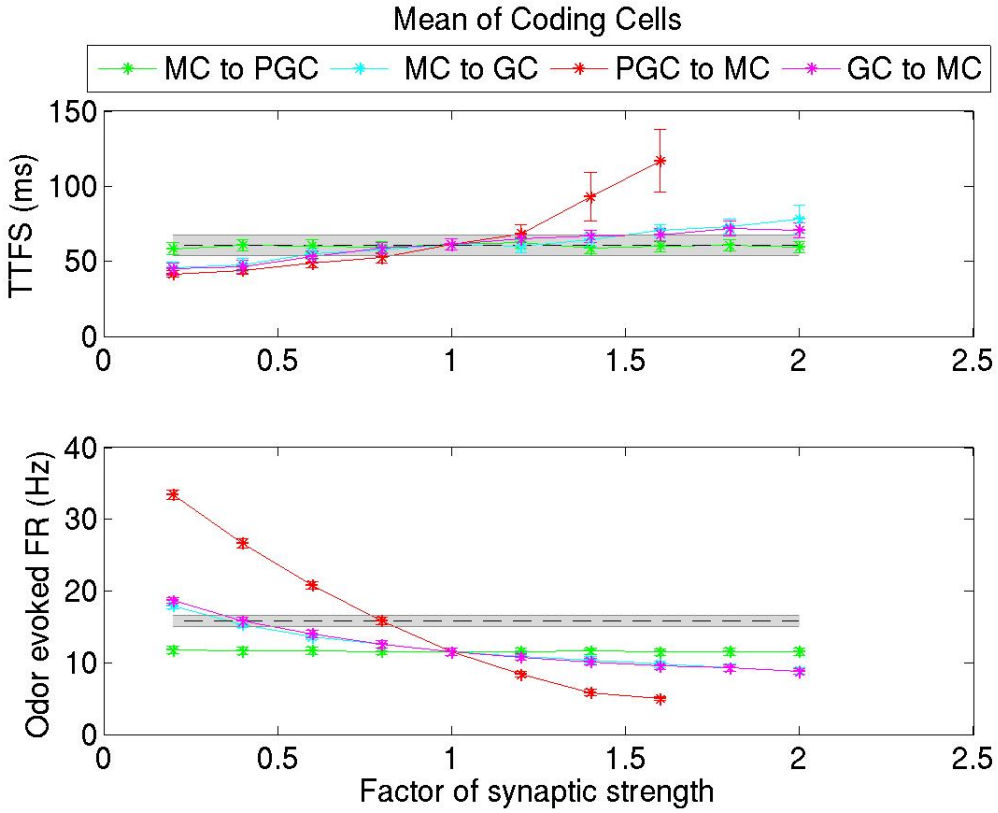

Response properties of coding cells. Top: Time-to-first spike (TTFS); Bottom: Odor-evoked firing rate (FR); X-axis: The scaling factors used to modify the synaptic strength; MC: mitral cell; PGC: periglomerular cell; GC: granule cell; Dashed lines: corresponding values of the tufted network; Asterisks: mean values from 30 trials. Errorbars and width of the gray area: standard error of the mean from 30 trials.

Figure 4.10: The effect in the response of the 13th cell while modifying the probability of connection between mitral and granule cells or the number of granule cells.

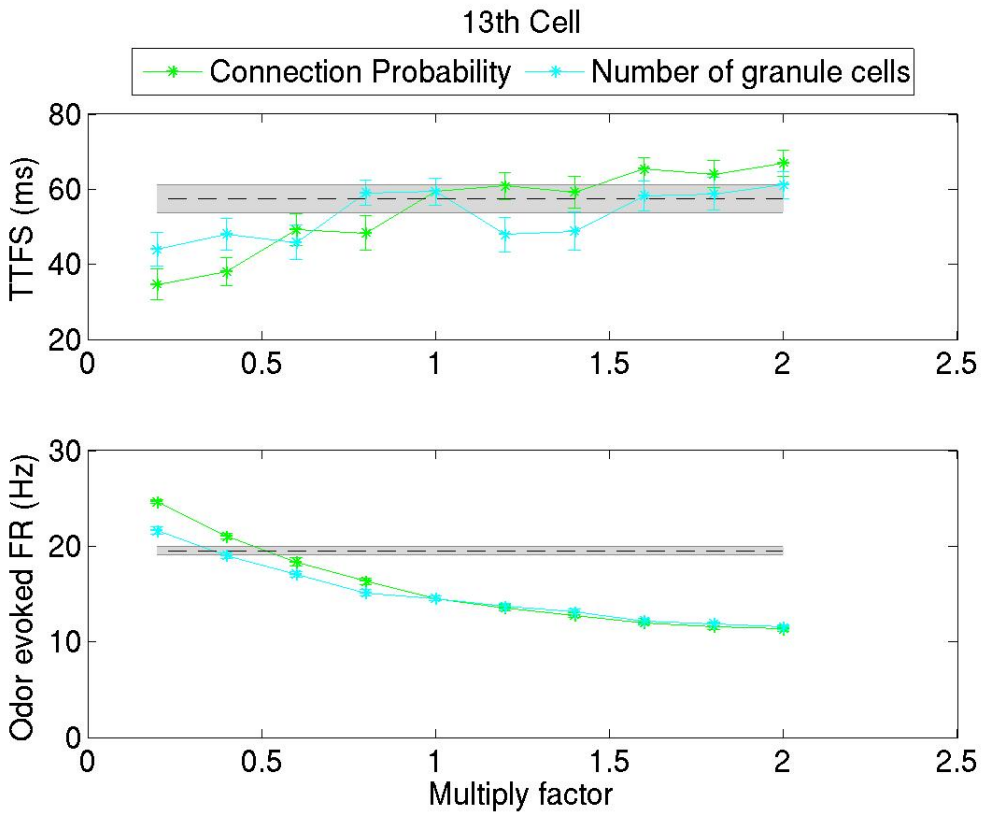

Response properties of the 13th cell. Top: Time-to-first spike (TTFS); Bottom: Odor-evoked firing rate (FR); X-axis: The scaling factors used to modify the initial probability of connection between granule and mitral cells (0.3) or the initial number of granule cells (100), represented by the green and blue lines respectively; Dashed lines: corresponding values of the tufted network; Asterisks: mean values from 30 trials. Errorbars and width of the gray area: standard error of the mean from 30 trials.

Figure 4.11: The effect in the response of coding cells while modifying the probability of connection between mitral and granule cells or the number of granule cell.

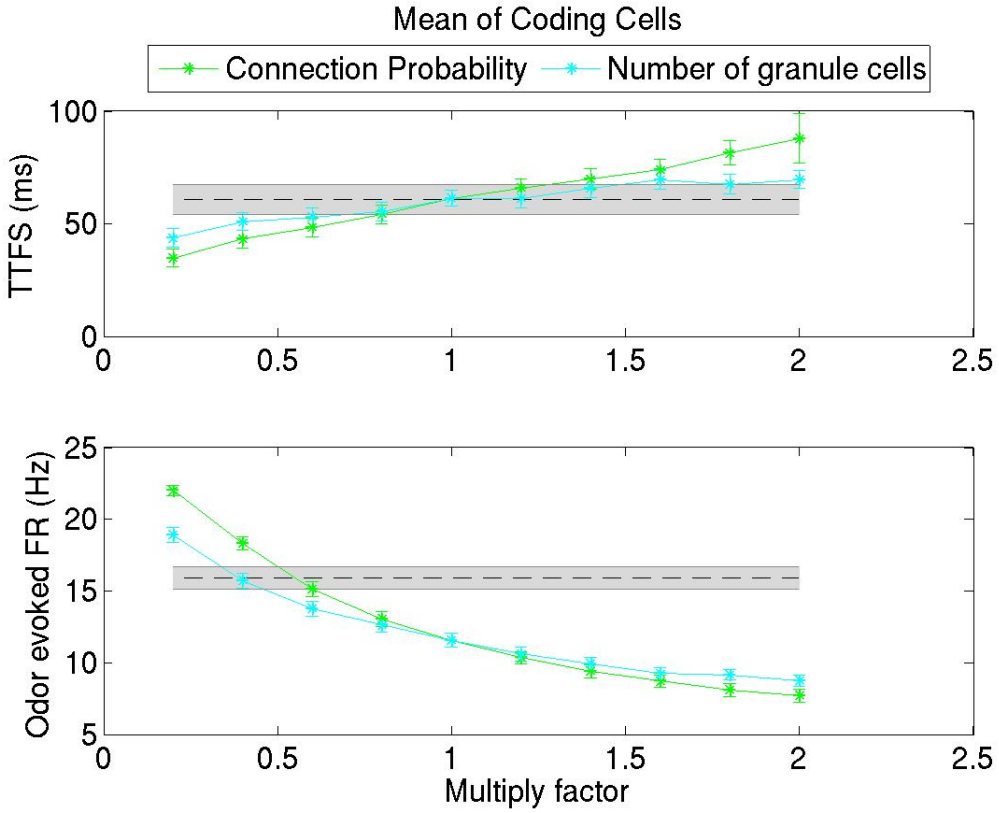

Response properties of coding cells. Top: Time-to-first spike (TTFS); Bottom: Odor-evoked firing rate (FR); X-axis: The scaling factors used to modify the initial probability of connection between granule and mitral cells (0.3) or the initial number of granule cells (100), represented by the green and blue lines respectively; Dashed lines: corresponding values of the tufted network; Asterisks: mean values from 30 trials. Errorbars and width of the gray area: standard error of the mean from 30 trials.

Figure 4.12: The effect in the response of the 13th cell while modifying the efficacy of the olfactory sensory neurons synaptic input to mitral or periglomerular cells.

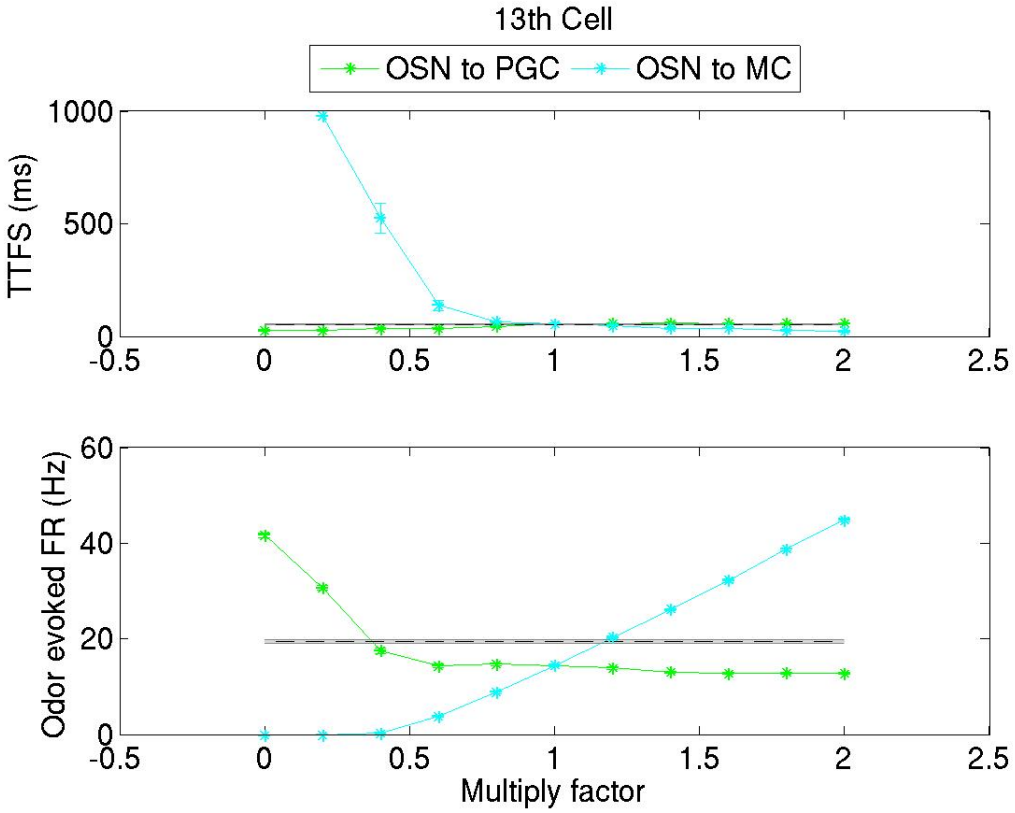

Response properties of the 13th cell. Top: Time-to-first spike (TTFS); Bottom: Odor-evoked firing rate (FR); X-axis: The scaling factors used to modify the odor-simulating current input into mitral (MC) or periglomerular (PGC) cells, represented by the green and blue lines respectively; Dashed lines: corresponding values of the tufted network; Asterisks: mean values from 30 trials. Errorbars and width of the gray area: standard error of the mean from 30 trials.

Figure 4.13: The effect in the response of coding cells while modifying the efficacy of the olfactory sensory neurons synaptic input to mitral or periglomerular cells.

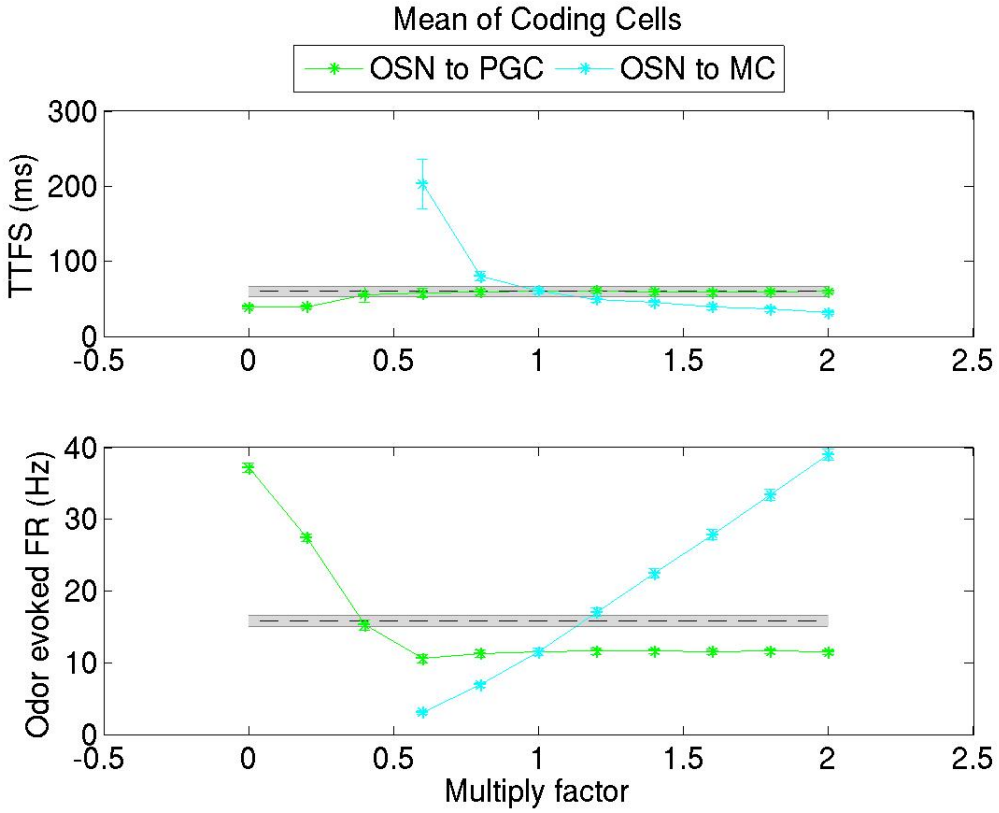

Response properties of coding cells. Top: Time-to-first spike (TTFS); Bottom: Odor-evoked firing rate (FR); X-axis: The scaling factors used to modify the odor-simulating current input into mitral (MC) or periglomerular (PGC) cells, represented by the green and blue lines respectively; Dashed lines: corresponding values of the tufted network; Asterisks: mean values from 30 trials. Errorbars and width of the gray area: standard error of the mean from 30 trials.

Overall, many network parameters were capable of modifying the response of mitral cells. Notably, modifications that caused a delay in the TTFS also caused a decrease in the FR_{ev}. Specifically, increasing the synaptic weight from periglomerular to mitral cells had a strong effect in both TTFS (increase) and FRev (decrease). A similar but smaller effect was observed by

decreasing the synaptic weight from mitral to granule cells or from granule to mitral cells.
Increasing the probability of connection between granule and mitral cells or the number of granule cells also delayed the TTFS and decreased the FR_{ev}. The effect of modifying the probability of connection was slightly stronger than modifying the number of granule cells.
Finally, modifying the efficacy of the odor-evoked current input into mitral or periglomerular cells also had a modulatory effect in the response properties. Decreasing the efficacy of odor input into mitral cells caused a delay of TTFS and a decrease in FR_{ev}, while increasing it caused mainly an increase in the FR_{ev}. As for the efficacy of the odor input into periglomerular cells, it only had an effect when decreased below baseline values and it mainly positively modulated the FR_{ev}.

4.2.3 The mitral and the tufted network

Next in our study, we concluded to two different networks, incorporating both biophysical and network differences, to represent the mitral and the tufted network. Although, in reality the divergence of the two networks arises most probably by the convergent effect of multiple parameters, we simplified our models by incorporating a minimal set of differences between the two networks. In order to achieve this, we run a large number of simulations (data not shown) both in the mitral and the tufted network, varying the most suitable of the above mentioned parameters. Based on that exhaustive search, we concluded to the parameters described bellow that reproduce many of the desired features.
From the set of the possible biophysical parameters we chose to incorporate a reduced conductance of primary dendrite Na_f in the mitral single cell network. Specifically this conductance was reduced to 20% of its initial value. This modification had a minimal effect in the single cells properties of the mitral cells, but led to a slightly increased TTFS. The modified biophysi-

cal properties of the mitral cell in comparison to its previous properties are presented in table 4.4.

We also differentiated two network parameters for the two networks. Specifically, in the mitral network the probability of connection between mitral and granule cells was multiplied by 1.5 and the weight of connection from granule to mitral cells by 1.75. These changes are realistic given the fact that the lateral dendrites of mitral cells are longer than those of tufted cells, resulting in higher connectivity between mitral and granule cells for the mitral network. Finally, we also doubled the effectiveness of the olfactory sensory neuron input to both mitral and tufted cells to better approximate reported values of odor-evoked firing rates.

The resulting network output properties for the two networks are shown in the figures 4.14 and 4.15, where M2 and T2 represent the mitral and the tufted network respectively. For comparison, we also present the properties of the mitral and tufted networks where the only difference between them was the different single cell models for mitral and tufted cells. We refer to these networks as M1 and T1 (mitral and tufted network respectively).

Figure 4.14 shows the time to first spike, spontaneous firing rate and the odor-evoked firing rate for these four networks for each one of the 25 cells. Figure 4.15 is a comparison of the same properties between these four networks for the 13^{th} cell and for coding cells. Errorbars represent the standard error of the mean from 30 trials.

	Mitral 1*	Mitral 2**
Passive properties		
Vrest (mV)	-59.07	-59.07
Rinput (MΩ)	74.62	74.45
τm (ms)	14.4	14.4
Cm (pF)	190.18	190.18
Sag amplitude (mV)	2.07	2.06
AP properties		
Vthreshold (mV)	-39.68	-42.9
Amplitude (mV)	74.77	74.24
FWHM (ms)	1.0714	1.15
AHP (mV)	28.09	24.47
$T_{AHP\ 50\ \%}$ (ms)	100.06	66.17
Sp. train properties		
Rheobase (pA)	90	90
RSL (ms)	774.9	1747.6
SL_{100pA}	388.3	759.8
FI curve gain (Hz)	7.5	8.5
$FR_{300\ pA}$ (Hz)	24.5	24

*Primary dendrite Na_f conductance $1 \cdot 10^{-4}$ S/cm^2.
**Primary dendrite Na_f conductance $0.2 \cdot 10^{-4}$ S/cm^2.

Table 4.4: Electrophysiological properties of mitral cell models.

Figure 4.14: Comparison of spontaneous FR, FR_{ev} and TTFS between four networks for each one of the 25 neurons.

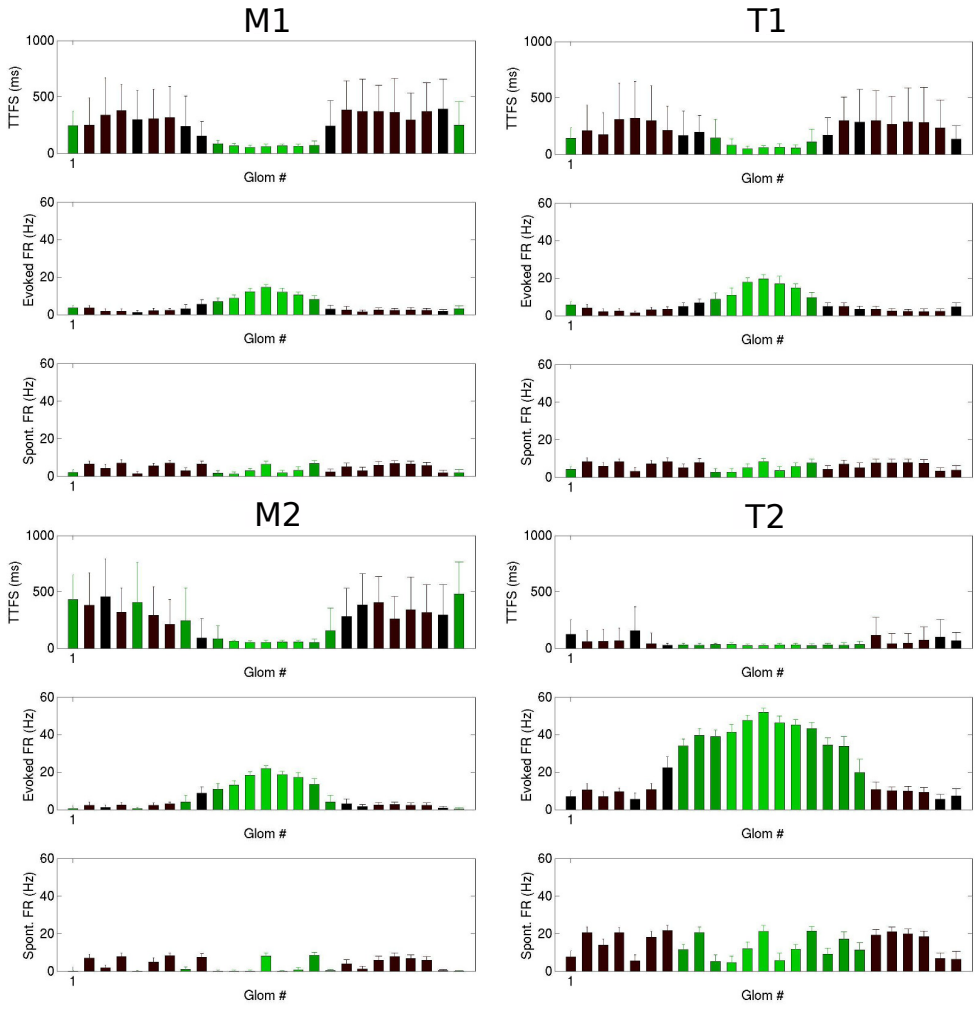

M1: the mitral network; T1: the tufted network; M2: the mitral network with doubled efficacy of input from olfactory sensory neurons to mitral cells, 1.75 times higher weight of connection from granule to mitral cells and 1.5 times higher probability of connection between mitral and granule cells; T2: the tufted network with doubled efficacy of input from olfactory sensory neurons to tufted cells; The three panels for each network present from top to bottom the time-to-first spike (TTFS), the odor-evoked firing rate (FR) and the spontaneous FR; X-axis: The 25 principal neurons (position-numbers of the corresponding glomeruli); Green bars: cells with significant increase in FR during odor input compared to spontaneous activity; Errorbars: standard deviation from 30 trials.

Figure 4.15: Comparison of spontaneous FR, FR_{ev} and TTFS for the 13^{th} and the coding cells of four networks.

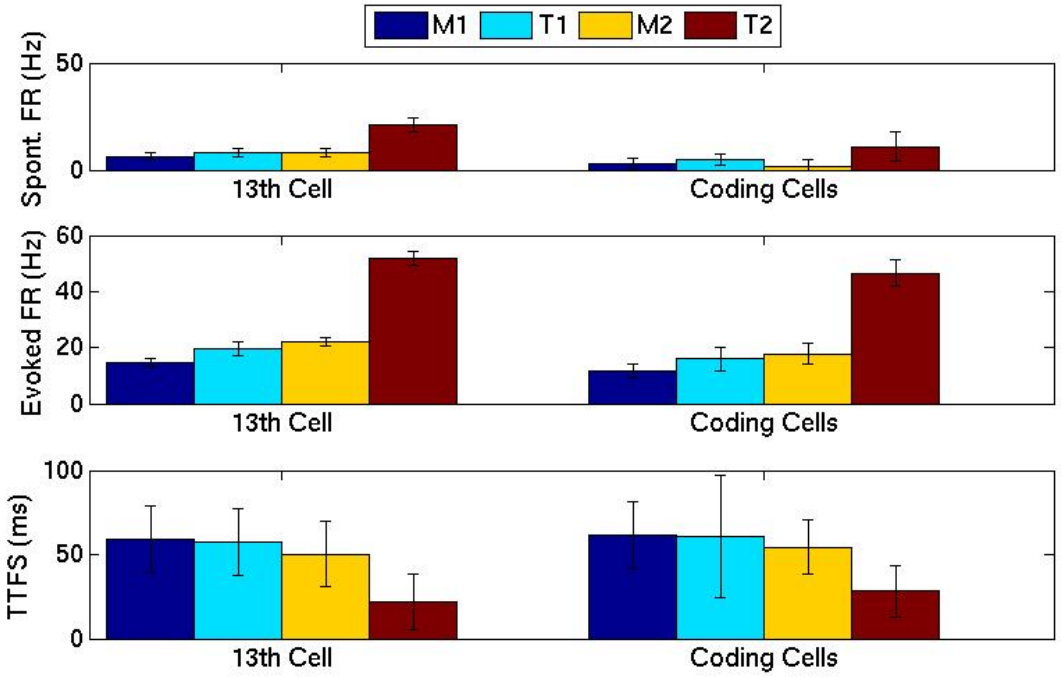

M1, T1, M2 and T2 as in figure 4.14; Top: Spontaneous firing rate (FR); Middle: Odor-evoked FR; Bottom: Time-to-first spike(TTFS); Left: Properties of the 13^{th} cell; Right: Properties of coding cells; Errorbars: Standard error of the mean for 30 trials.

4.3 Part C: Information coding by the parallel networks

In this last part of our study, we aimed to evaluate the coding mechanisms of the two output networks of the olfactory bulb. We used the two model networks to investigate possible mechanisms of each network for coding for odor molecule concentration and for differentiating similar odors. Again we

evaluated the network output by examining the firing rate and the TTFS of the output neurons.

4.3.1 Coding for concentration

We modelled the increasing concentration of the same odor by multiplying the amplitude of the current input into each principal neuron by a constant factor. This way the relative amplitude between glomeruli remained constant. Figure 4.16 shows the input current for each cell while increasing or decreasing the concentration.

Figure 4.16: Odor-simulating input in each of the 25 cells while changing odor concentration.

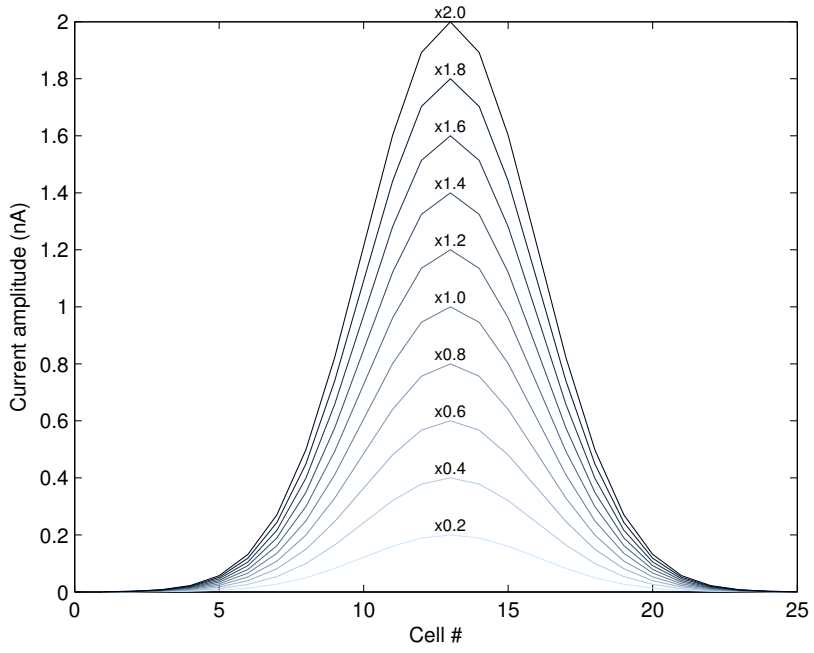

Figures 4.17 - 4.20 show the effect of changing concentration in the response of principal neurons. We evaluated the effect of relatively lower and higher concentrations separately. We focused again in the FR_{ev} and the TTFS.

Figure 4.17: Response of 13$^{\text{th}}$ cell while increasing odor concentration (low concentrations)

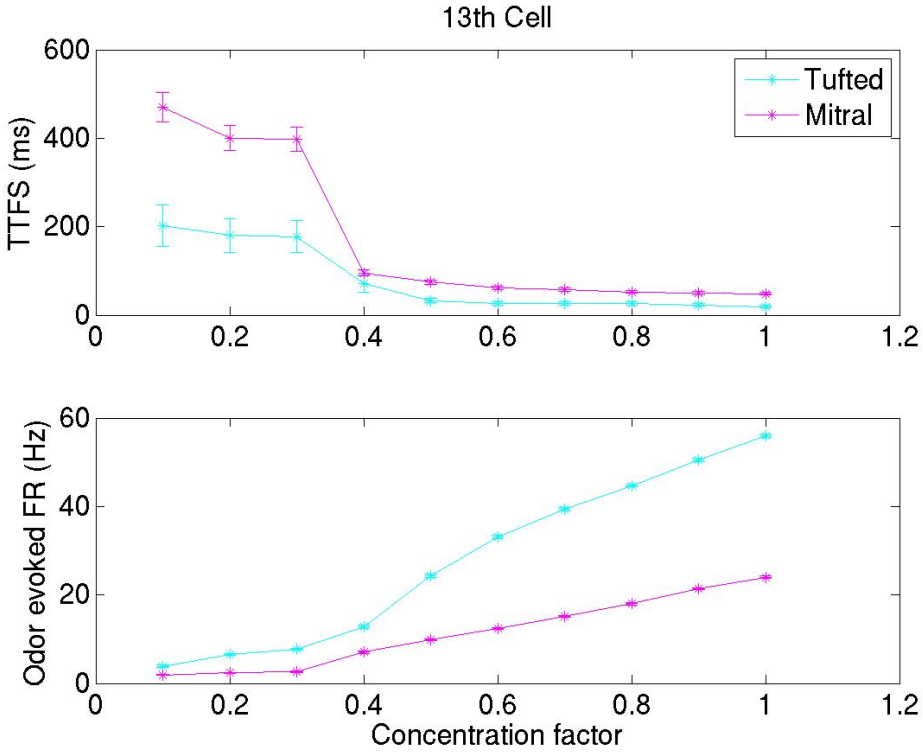

Response properties of the 13$^{\text{th}}$ cell. Top: Time-to-first spike (TTFS); Bottom: Odor-evoked firing rate (FR); X-axis: The scaling factors used to uniformly modify the odor-simulating current input into each one of the principal neurons; Magenta: Properties of the mitral network; Blue: Properties of the tufted network; Asterisks represent the mean values and errorbars the standard error of the mean from 30 trials.

Figure 4.18: Response of coding cells while increasing odor concentration (low concentrations)

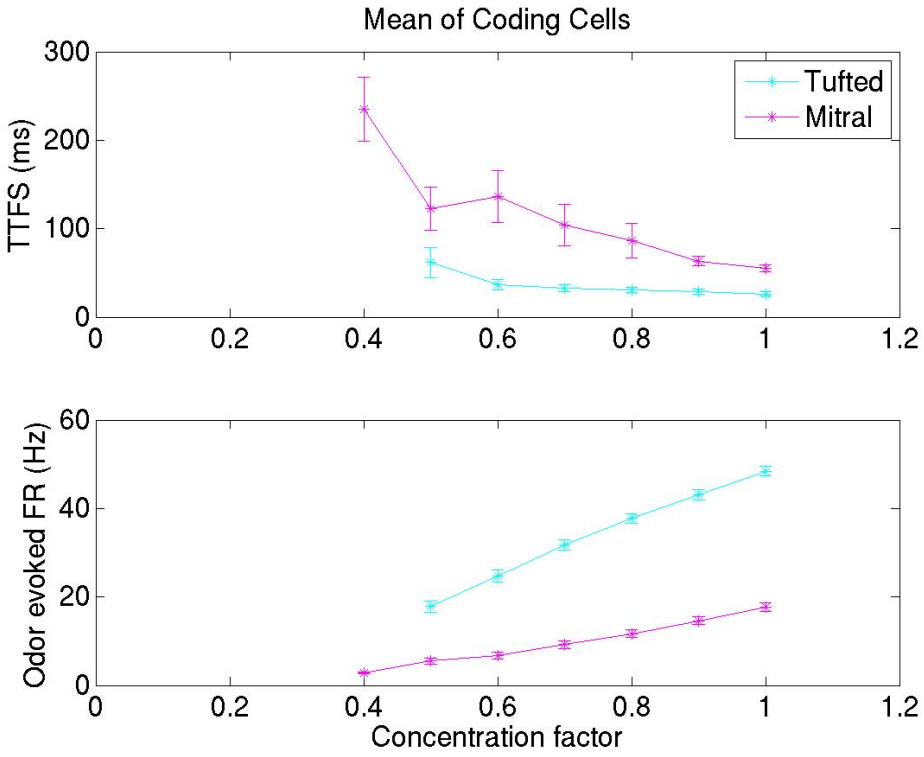

Response properties of coding cells. Top: Time-to-first spike (TTFS); Bottom: Odor-evoked firing rate (FR); X-axis: The scaling factors used to uniformly modify the odor-simulating current input into each one of the principal neurons; Magenta: Properties of the mitral network; Blue: Properties of the tufted network; Asterisks represent the mean values and errorbars the standard error of the mean from 30 trials.

Figure 4.19: Response of 13$^{\text{th}}$ cell while increasing odor concentration (high concentrations).

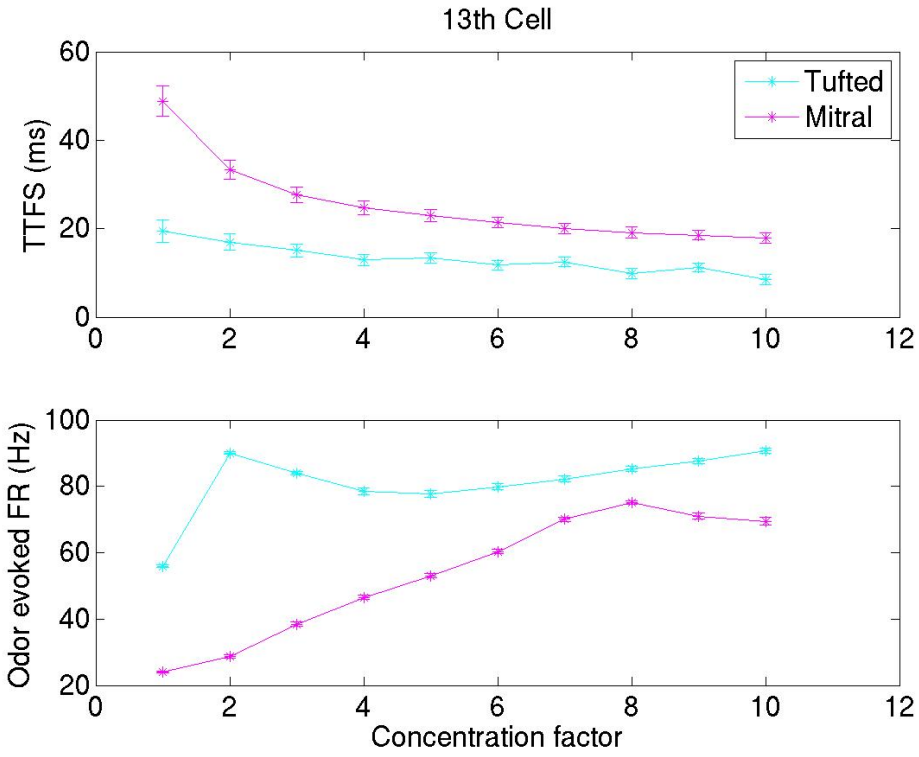

Response properties of coding cells. Top: Time-to-first spike (TTFS); Bottom: Odor-evoked firing rate (FR); X-axis: The scaling factors used to uniformly modify the odor-simulating current input into each one of the principal neurons; Magenta: Properties of the mitral network; Blue: Properties of the tufted network; Asterisks represent the mean values and errorbars the standard error of the mean from 30 trials.

Figure 4.20: Response of coding cells while increasing odor concentration (high concentrations).

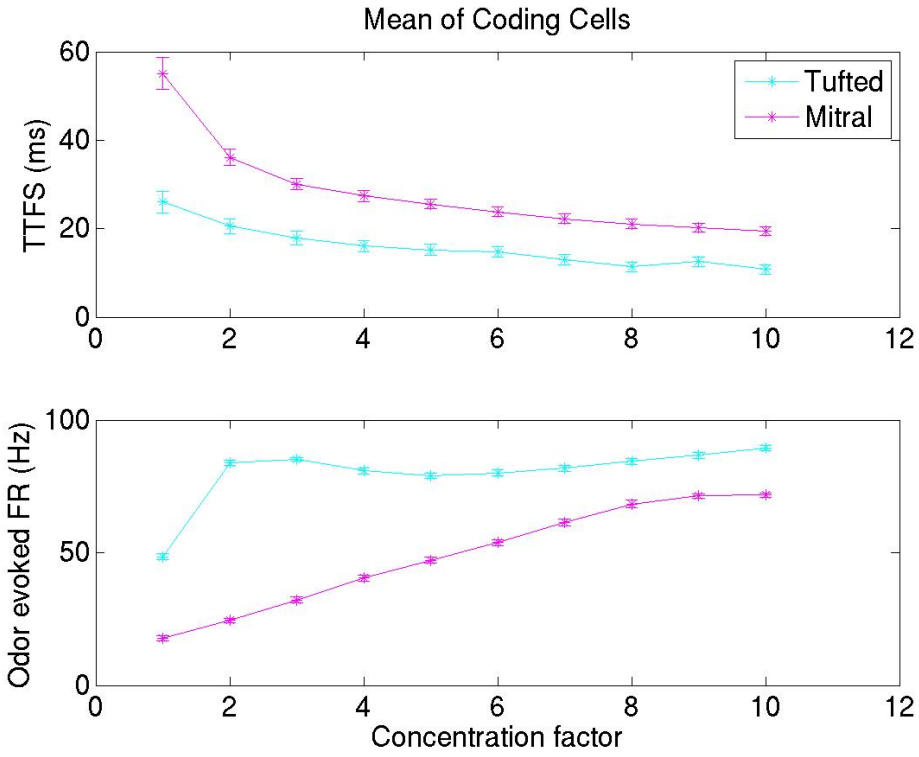

Response properties of coding cells. Top: Time-to-first spike (TTFS); Bottom: Odor-evoked firing rate (FR); X-axis: The scaling factors used to uniformly modify the odor-simulating current input into each one of the principal neurons; Magenta: Properties of the mitral network; Blue: Properties of the tufted network; Asterisks represent the mean values and errorbars the standard error of the mean from 30 trials.

Overall, at concentrations below 40% of the baseline, increasing the concentration causes a decrease in the TTFS for both mitral and tufted cells. Also, there is a slight increase in the FR_{ev} mainly of tufted cells. At higher concentrations (40-200%), however, the TTFS remains largely concentration invariant, while the FR_{ev} increases for both cell types. At very high concentrations (>200%), we observe an increase mainly in the FR_{ev} of mitral cells. At all concentration, TTFS of tufted cells is constantly longer and

FR_{ev} constantly higher than the corresponding properties of mitral cells.

4.3.2 Differentiating similar input patterns

To investigate possible mechanisms of differentiating similar odors we evaluated the output of the network after stimulation with four different input patterns. Odor1 had the highest affinity for the 13^{th} cell, odor2 for the 16^{th} cell and odor3 for the 6^{th} cell. We also stimulated the two networks with a higher concentration of odor1 (high odor1) with double maximum current amplitude. Figure 4.21 shows the amplitude of the current input into each one of the network output cells for odor1, odor 2 and odor 3. The corresponding curve for high odor1 is the highest curve in figure 4.16.

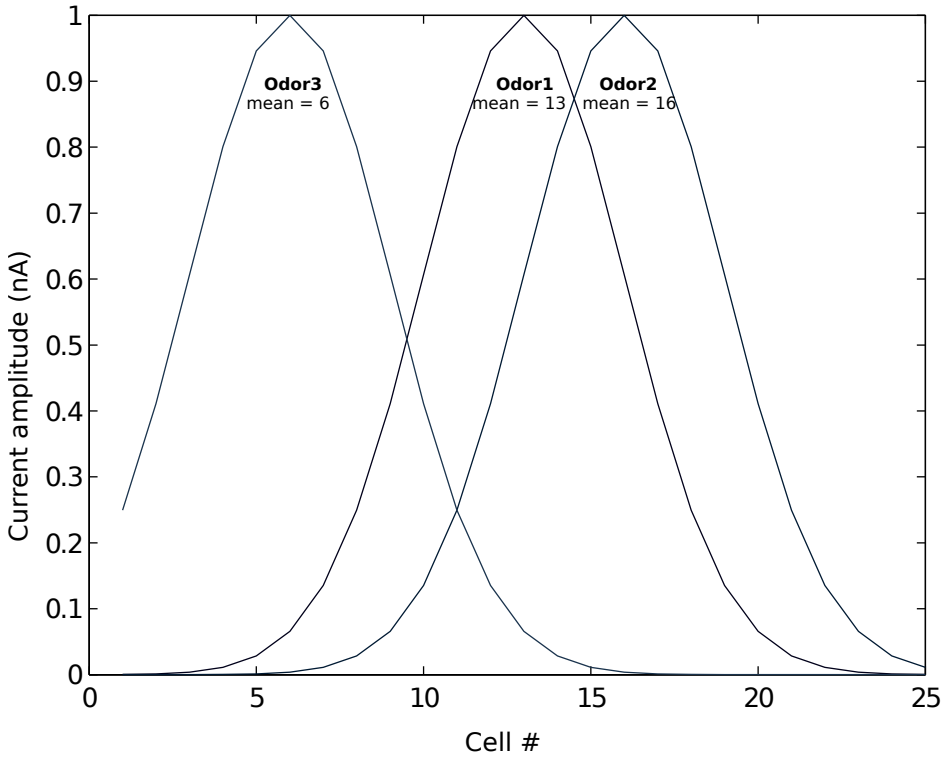

Figure 4.21: Different odors represented by different input distributions across the projection neuron population.

Figures 4.22 - 4.27 show the response properties of each network when simulated with different (odor2 / odor3) or similar (odor1 / odor2) odors. We also compare the response after stimulating the network with similar odors at different concentrations (high odor1 / odor2). The upper plot in each figure shows the TTFS for coding cells (values of non-coding cells have been removed for clarity) and the lower plot shows the FR_{ev} for each of the 25 cells. This way these figures demonstrate both spatial (number of coding cells) and temporal (TTFS, FR_{ev}) coding properties of the two networks. Shaded areas represents standard error of the mean from 30 trials.

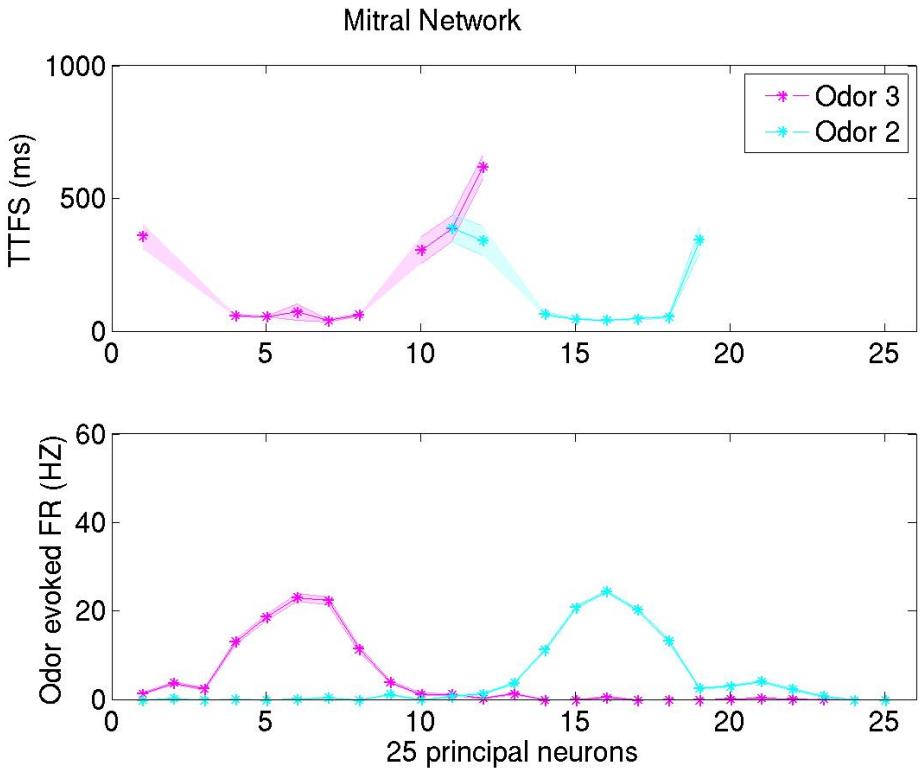

Top: Time-to-first spike (TTFS); Bottom: Odor-evoked FR; X-axis: the 25 principal neurons; Magenta plots: Responses after stimulation with odor 3 input pattern; Blue plots: Responses after stimulation with odor 2 input pattern; Asterisks represent the mean values and shadows the standard error of the mean from 30 trials.

Figure 4.22: Mitral network - coding for different odors.

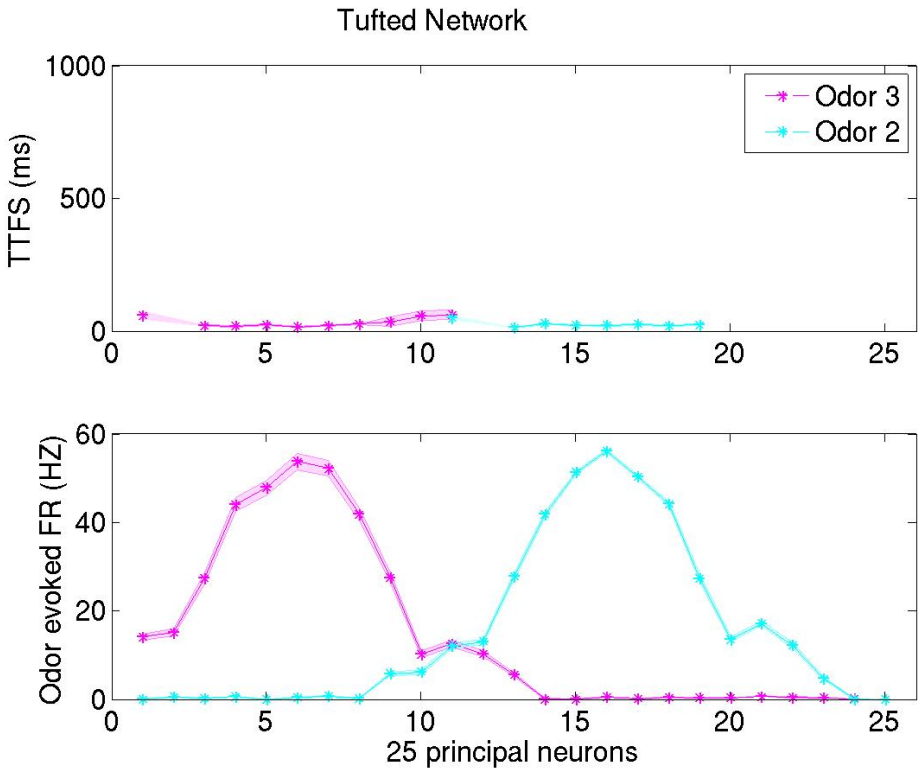

Top: Time-to-first spike (TTFS); Bottom: Odor-evoked FR; X-axis: the 25 principal neurons; Magenta plots: Responses after stimulation with odor 3 input pattern; Blue plots: Responses after stimulation with odor 2 input pattern; Asterisks represent the mean values and shadows the standard error of the mean from 30 trials.

Figure 4.23: Tufted network - coding for different odors.

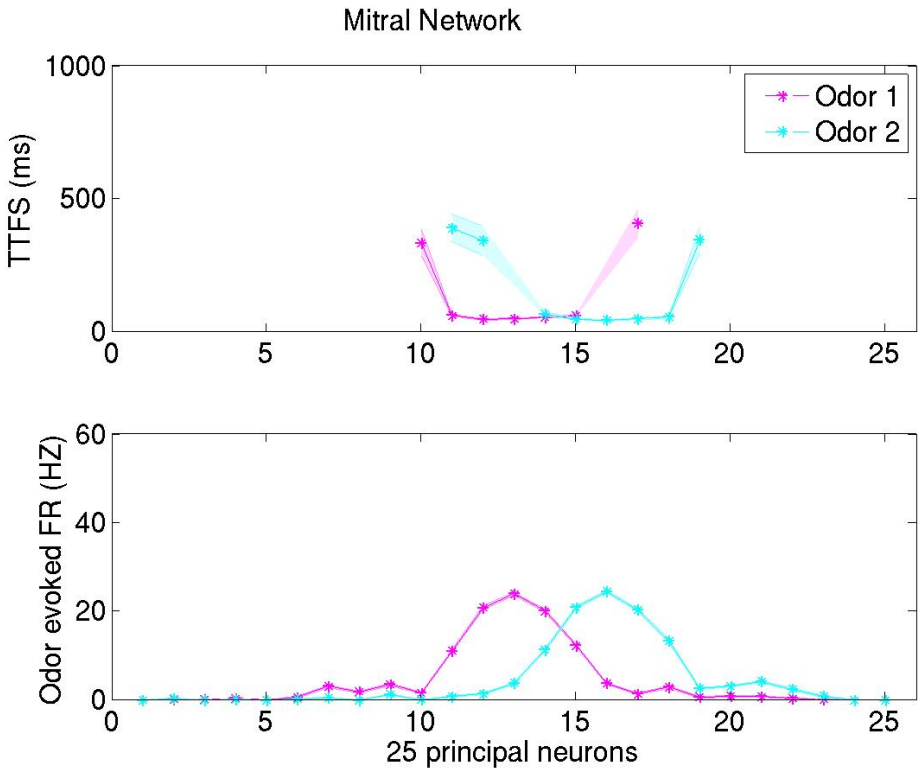

Top: Time-to-first spike (TTFS); Bottom: Odor-evoked FR; X-axis: the 25 principal neurons; Magenta plots: Responses after stimulation with odor 1 input pattern; Blue plots: Responses after stimulation with odor 2 input pattern; Asterisks represent the mean values and shadows the standard error of the mean from 30 trials.

Figure 4.24: Mitral network - coding for similar odors.

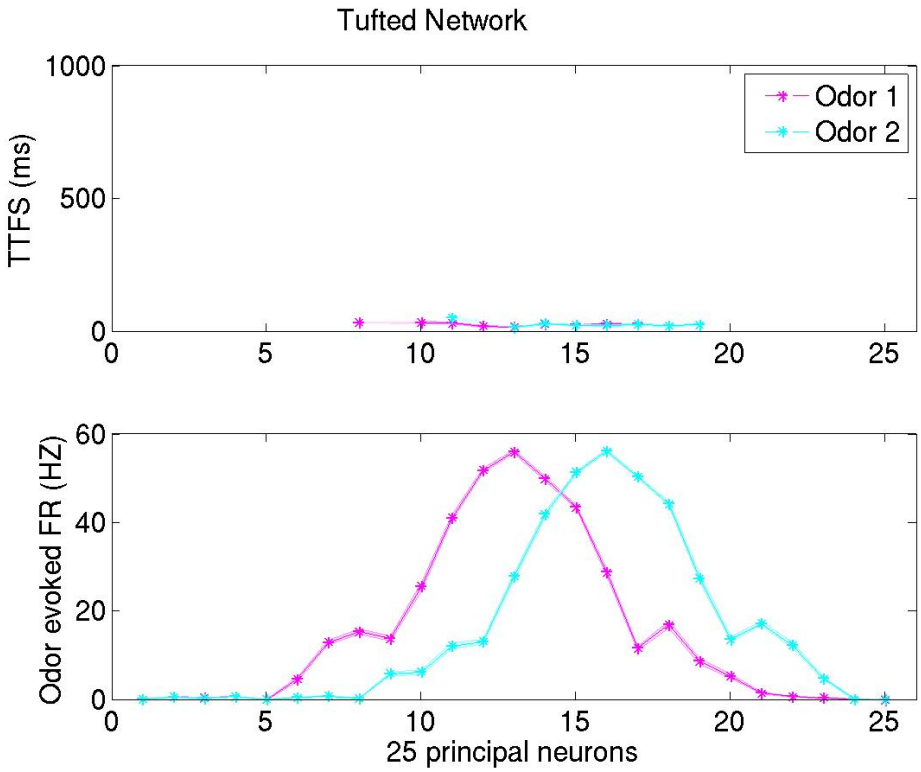

Top: Time-to-first spike (TTFS); Bottom: Odor-evoked FR; X-axis: the 25 principal neurons; Magenta plots: Responses after stimulation with odor 1 input pattern; Blue plots: Responses after stimulation with odor 2 input pattern; Asterisks represent the mean values and shadows the standard error of the mean from 30 trials.

Figure 4.25: Tufted network - coding for similar odors.

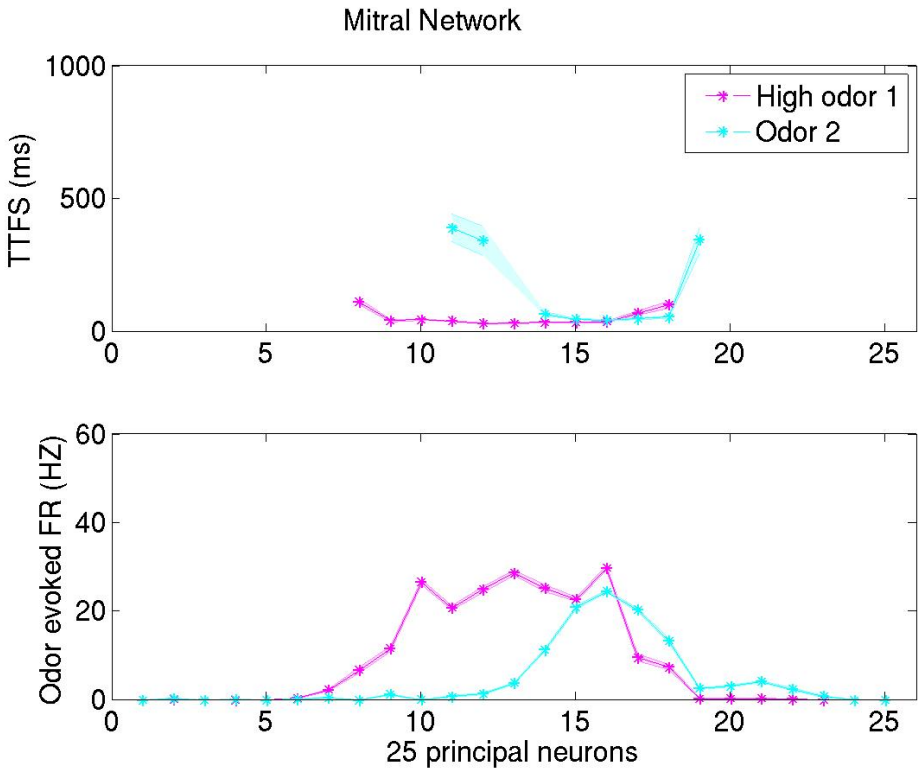

Top: Time-to-first spike (TTFS); Bottom: Odor-evoked FR; X-axis: the 25 principal neurons; Magenta plots: Responses after stimulation with a higher concentration of odor 1; Blue plots: Responses after stimulation with odor 2; Asterisks represent the mean values and shadows the standard error of the mean from 30 trials.

Figure 4.26: Mitral network - coding for similar odors at different concentrations.

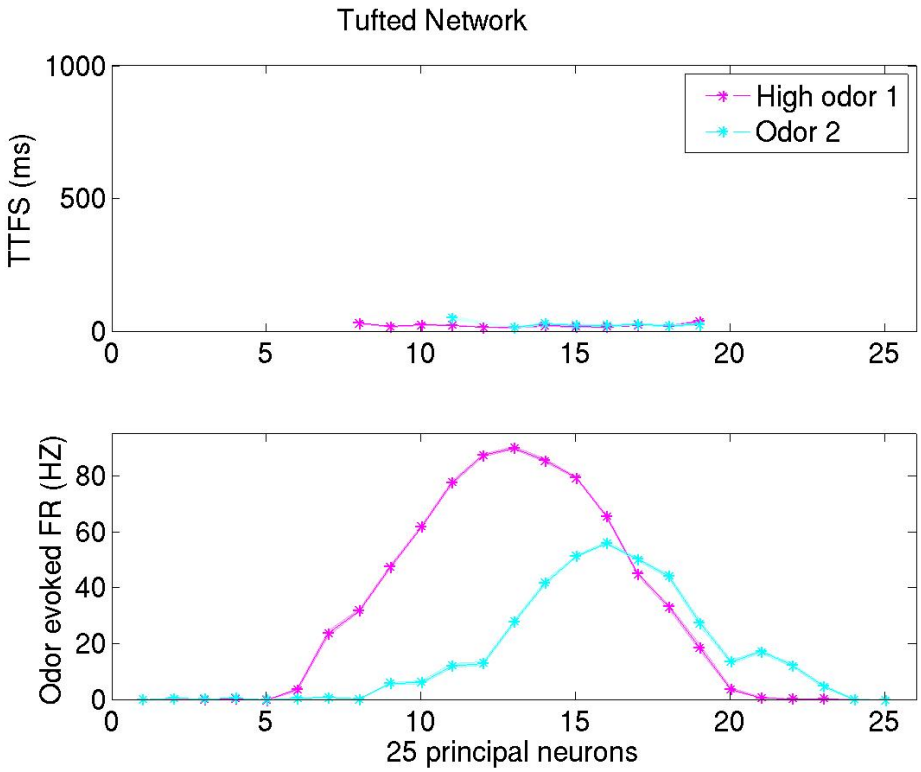

Top: Time-to-first spike (TTFS); Bottom: Odor-evoked FR; X-axis: the 25 principal neurons; Magenta plots: Responses after stimulation with a higher concentration of odor 1; Blue plots: Responses after stimulation with odor 2; Asterisks represent the mean values and shadows the standard error of the mean from 30 trials.

Figure 4.27: Tufted network - coding for similar odors at different concentrations.

Overall, both networks demonstrate distinct responses when stimulated with different input patterns. Specifically, for both networks the populations of coding cells are distinct for different input patterns. When simulated with similar input patterns, the response patterns of the tufted network are highly overlapping. The main distinguishing property is the position of the mitral cell that responds with the highest FR_{ev}. On the other hand, the responses of the mitral network can be distinguished by the distinct populations of coding cells that respond with short latency. The response patterns of the mitral network are separable even when stimulated with similar input patterns at

different concentrations. Specifically, for the lower-concentration input, the number of coding cells with fast responses is smaller compared to the one corresponding to the higher-concentration input. For the tufted network, the main distinguishing properties of the response patterns to similar odors at different concentrations are the maximum FR_{ev} and the postition of the tufted cell that responds with the highest FR_{ev}. The populations of fast-responding coding cells, however, is rather overlapping. For all simulations, the FR_{ev} of tufted cells are constantly higher and the population of coding cells is constantly bigger compared to mitral cells.

5 | Discussion

What is the role of these parallel pathways conveying odor-related information? First of all, the olfactory system is a rather demanding sensory system given the huge odor molecule repertoire. The difficulty of the tasks undertaken by the olfactory system grows with the need to code for evolving stimulus representations. In this case the olfactory system needs to code for the new features of the stimulus independently of the previous on-going representation. What is more, it must independently code for opposite features of an odor representation. For example, it is responsible for the encoding and perception of both the concentration of an odorant (concentration coding) and the odor identity regardless of the concentration (concentration invariance). Coding of concentration is essential for tracking the source of the odorants and concentration invariance is important so as for odor identity perception to be stable within a wide range of stimulus concentrations. What is more, depending on the task on demand, it must be able to both group and differentiate similar odors. Such contradictory coding features could be computed by different microcircuits and conveyed by distinct pathways and are possible functional roles for the parallel pathways of mitral and tufted cells.

A first step in understanding the different functional roles of mitral and tufted cells is to elucidate the mechanisms generating their distinct responses. In our study, we took advantage of the opportunities of computational modeling to design experiments for the systematic exploration of the effect of single cell and network parameters in the response properties of principle neurons. This way we identified possible mechanisms generating their distinct response properties. Increased firing frequencies of tufted cells were correlated with their higher intrinsic excitability. Increased response latency of mitral cells could be generated by increased feedforward and feedback inhibition and to a lesser extent by modifying biophysical parameters.

We also examined the functional implications of the distinct response properties by comparing the response patterns of a mitral and a tufted network after stimulation with different input amplitudes and with similar input patterns. Overall, the response of the tufted network was spatially more limited and temporally more delayed. On the other hand the tufted network responded faster with higher firing rates and wider spatial activation. These findings are consistent with the view that tufted cells are responsible for faster coding of generalized signals, while mitral cells for inevitably delayed coding of better processed signals.

5.1 Differences between the mitral and the tufted cell models

In the first part of this study we modelled the tufted and mitral cells based on reported differences in their intrinsic biophysical properties and in their responses to somatic current injections (Burton and Urban, 2014). The main characteristics we tried to match were the different action potential traces (duration of the action potential, duration of afterhyperpolariation), the different levels of intrinsic excitability (differences in firing rates after somatic current injections) and the different degree of firing irregularity between mitral and tufted cells. After developing a satisfactory pair of a mitral and a tufted cell, we further systematically changed many of their biophysical properties to achieve further improved models. The final models demonstrate the main differences presented by the experimental study of Burton and Urban (2014) (table 4.3).

One of the main differences between our model data and the experimental data is the increased amplitude of the AHP for both the mitral and the tufted cell model. Manipulations of all conductances of ionic channels (including K_{CA} that is known to modulate the amplitude of AHP) did not improve this discrepancy. It is possible that the AHP model used here does not cap-

ture all aspects of this current in olfactory bulb neurons and a better model would solve this problem. However, due to the lack of experimental data we were not able to develop a better model for the AHP current. With this AHP model, the only biophysical manipulation that caused a decrease in the amplitude of AHP was the elevation of K^+ reverse potential. Although we found no reported data of this property for olfactory bulb principal neurons, we chose not to increase it to values higher than -70 mV, in order to remain within biologically accepted values. Nevertheless, we consider that this difference will not have a significant effect in the odor-evoked firing properties of mitral and tufted cells, especially since the duration of AHP is within the experimentally reported values.

The following table summarizes the distinct biophysical properties attributed to the mitral and the tufted model in order to achieve the reported differences.

	Mitral	Tufted
Passive properties		
Morphology factor**	1.2	0.95
Membrane resistance ($\Omega \cdot cm^2$)	$30 \cdot 10^3$	$18 \cdot 10^3$
Coductances of ionic channels*		
Na_p	0.14	1.1
K_{DR}	0.2	1.2
K_s	0.12	1
K_{Ca}	5	1
LCa	1	0.1
I_h channels	1	2

* Factor uniformly multiplying diameter and length of all compartments.
** Multiply factor for the baseline values of table 3.3. For the I_h channels baseline values are the values of the mitral cell model (table 4.1).

Table 5.1: Comparison of biophysical properties between the two models.

5.2 Possible mechanisms for the distinct response properties to afferent signals

Although, the existence of anatomical and synaptic differences between mitral and tufted principal neurons are known for years there are still many gaps to fill with regard to their intrinsic biophysical and synaptic differences. What is more, the correlation of such differences with the distinct response properties of mitral and tufted cells after odor stimulation remains elusive. Below we summarize the possible differentiating mechanisms and their correlation with the distinct response properties based on our findings and on literature data.

5.2.1 Differences in intrinsic biophysical properties

In the study of Burton and Urban (2014) it was shown that mitral and tufted cells differ significantly in their intrinsic excitability. This difference will inevitably result in different strength of the response to afferent-evoked stimulation. Authors of this study speculate that differences in excitability could arise from differences in voltage-gated potassium channel properties. In our study we concluded that the difference in excitability can indeed result from differences in intrinsic biophysical properties. Specifically, in our models, the increased conductance of Na_p channels caused increased intrinsic excitability compared to mitral cells. This initial difference in excitability can be enhanced by synaptic mechanisms.

On the other hand, differences in the response latency seem to better correlate with differences in the mitral versus tufted network properties, although, differences in biophysical properties of single neurons also contribute to some extent. In our study we found a positive correlation between the conductance of K_A in the primary (and to a less extent in the lateral) dendrite and the response latency (figures 4.2, 4.3, 4.6, 4.7). However, these manipulations

modified the values of the passive electrophysiological properties outside the experimentally reported range (data not show). Decreasing the conductance of Na_f also increased the response latency without considerable alternations in the electrophysiological properties. The effect, however, was quite small.

5.2.2 Differences in synaptic properties

5.2.2.1 Differences in inhibitory circuits

Differences in inhibitory circuits include connecting with different subtypes of interneurons, different connectivity dynamics with the same interneurons and different pathways that construct the circuits of the mitral and the tufted subpopulations. Given the large number and types of interneurons and subtypes of interneurons in the olfactory bulb, these parameters most probably have an important effect in modulating the response of principal neurons. In the next paragraphs we discuss the parameters for which there is some evidence regarding a modulatory effect.

Connection with different types of granule cells Mitral and tufted cells are known to form dendrodendritic synapses with different subtypes of granule cells (Imamura et al., 2006, Shepherd et al., 2004). Although this could account for their different response properties, the exact correlation have not been investigated. In our study we approach this matter by systematically modifying the weight of connectivity between mitral and granule cells (figures 4.8, 4.9). We found that increasing the weight of connectivity from mitral to granule or from granule to mitral cells causes an observable increase in TTFS and decrease in odor-evoked firing rate, more evident in the coding cell population (figure 4.9). However, this effect is undermined by the more robust effect of changing the weight of connection from periglomerular to mitral cells.

Differences in the level of feedback inhibition Lateral inhibition is a form of feedback inhibition where an excited neuron inhibits the activity of neighbouring neurons. Mitral cells have been shown to receive stronger lateral inhibition compared to tufted cells (Christie et al., 2001, Nagayama et al., 2004). This is most probably mediated through their longer lateral dendrites that allow more synapses with granule cells. Authors of (Nagayama et al., 2004) speculate that the role of dendrodendritic synapses between tufted and granule cells is not the lateral inhibition but rather the determination of the phase preference in relation to respiratory rhythm.
Our experiment of modifying the weight of connectivity from granule to mitral cells examines the effect of feedback inhibition. As we mentioned above, increasing this weight had a relative small but observable effect in both TTFS and FR_{ev}. It would be interesting to reevaluate our data and examine the effect of this manipulation in the phase locking with regard to the sniff rhythm and in the extent of lateral inhibition. What is more, we evaluated the effect of the number of synapses between mitral and granule cells by systematically modifying both the total number of granule cells and the probability of connection between mitral and granule cells (figures 4.10, 4.11). Increased probability of connection can lead to increased delay of TTFS in the range of tenths of ms and to a small decrease in the FR_{ev}.
Periglomerular interneurons also mediate feedback inhibition. They are excited by activated principal neurons through their dendrodendritic synapses and subsequently, they cause feedback inhibition to the neurons that activated them. What is more, all periglomerular cells in our study are also excited by afferent inputs and therefore, they also mediate feedforward inhibition. Their contribution in the response properties is discussed in the next paragraph.

Differences in the level of feedforward inhibition Feedforward inhibition of olfactory bulb principal neurons is mainly mediated in the glomerular

layer. Mitral cells have been considered to receive stronger feedforward inhibition, presumably by periglomerular cells. In the study of Fukunaga et al. (2012) the authors speculate that the difference in the preferential firing phase between mitral and tufted cells is caused by differences in inhibitory networks and using computational models they conclude that it is probably mediated by differences in the afferent-evoked inhibition from periglomerular cells. Burton and Urban (2014) also consider an association of their finding of increased subthreshold responses of mitral cells after sequential stimulation cycles with increased afferent-evoked inhibition, possibly by periglomerular cells. We evaluated this hypothesis by systematically changing the strength of reciprocal dendrodendritic connections between mitral and periglomerular cells (figures 4.8, 4.9). We show that increased connectivity strength from periglomerular to mitral cells can indeed increase the TTFS, while also decreasing the FR_{ev}.

5.2.2.2 Differences in afferent-evoked excitation

This investigation includes both differences in the strength and differences in the pathway of excitatory input from olfactory sensory neuron to principal neurons of the olfactory bulb. Recent studies have demonstrated that tufted cells receive more effective monosynaptic input from olfactory sensory neurons, while mitral cells are mainly excited by an indirect pathway (Burton and Urban, 2014, Gire et al., 2012). What is more, in the computational part of the study of Fukunaga et al. (2012) it is shown that the strength of the input from olfactory sensory neurons to principal neurons can affect the phase difference between mitral and tufted cells. In the study of Burton and Urban (2014) authors state that the higher afferent-evoked firing rates of tufted cells could be partially caused by the more effective afferent-evoked excitatory input. However, they mainly correlate them with differences in intrinsic biophysical properties. In our results we show that the strength of the input from olfactory sensory neurons to mitral cells can affect both the

TTFS and the FR_{ev} of coding neurons (figures 4.12, 4.13).

5.2.2.3 Differences in neuromodulatory inputs

The circuits of the olfactory bulb are shaped by the activity of cortical and subcortical centrifugal neuromodulatory inputs. Subcortical modulation is mediated by cholinergic, adrenergic or serotonergic terminals that are speculated to affect the responses of the olfactory bulb circuits. However, the exact mechanisms and functional correlations have not been elucidated yet. Neuromodulatory inputs in the olfactory bulb are likely to enhance the differentiation of the responses between mitral and tufted cells. Such differentiating effect of subcortical inputs was recently proven by a study that investigated the effect of activating the serotoninergic raphe nuclei on the response of olfactory bulb principal neurons (Kapoor et al., 2016). In this study it was shown that raphe nuclei activation leads to potentiation of the already stronger response of tufted cells to odor stimulation. On the other hand, the effect on mitral cell response was bidirectional (excitatory or inhibitory) in a way that enhanced the separation of odor representations. However, they also showed that the effect of these inputs to both mitral and tufted principal neurons is most likely mediated through polysynaptic pathways. Given the fact that external tufted interneurons express receptors for serotonine, they speculate that direct neuromodulatory input into these interneurons activates local excitatory or inhibitory circuits that subsequently modulate the response of mitral and tufted cells. We can conclude that signals from raphe nuclei act on the differently wired circuits of mitral and tufted cells and cause differential modulation and further enhancement of the distinct response properties of principal neurons.

5.2.3 Summary of mechanisms that differentiate mitral from tufted cells and networks

All in all, the increased firing rates of tufted vs mitral cells is initially generated by differences in intrinsic biophysical properties. Tufted cells are in general intrinsically more excitable than mitral cell. However, differences in excitatory and inhibitory circuits also contribute to the observed differences in the afferent-evoked firing rates between principal neurons.
On the other hand differences in the response latency seem to be more strongly associated with differences in synaptic properties. Authors of (Burton and Urban, 2014) speculate that the different latencies of firing could be attributed to the combination of the differences in intrinsic excitability and in afferent-evoked excitation and inhibition. In addition to these parameters, feedback inhibitory inputs and cortical and subcortical inputs could also contribute to this phenomenon. In our study, however, we have shown that differences in intrinsic biophysical properties are also capable of generating observable differences in the response latency. It is intriguing to speculate that a small initial difference in the response latency and/or the different intrinsic excitability between the two populations might facilitate synaptic differences that lead to the significant difference in the temporal response between mitral and tufted cells.

5.3 Distinct functional role for mitral and tufted subpopulations

Each principal neuron of the olfactory bulb is related with a specific glomerulus, receiving input mainly from a specific population of olfactory receptor neurons. This means that sister mitral and tufted cells (dendritic tuft located in the same glomerulus) receive the same information. However, given the differences in their intrinsic and network properties, the two cell types seem

to process this information in different ways. What is more, distribution of the axon collaterals to the olfactory cortex has been shown to differ between the two cell types (Igarashi et al., 2012, Nagayama et al., 2010). Tufted cells have been shown to project only to anterior regions of the olfactory cortex, in contrast to mitral cells whose axons project to both anterior and posterior areas of the olfactory cortex (Igarashi et al., 2012). These differences imply that mitral and tufted cells have distinct functional roles. Although these distinct roles have not been elucidated yet, many interesting suggestions have been expressed.

5.3.1 Coding for concentration

In the study of Igarashi et al. (2012) it was shown that decreasing odor molecule concentration causes an increase in the firing latency of both mitral and tufted cells, while in the study of Fukunaga et al. (2012) that it causes a phase advance only in mitral cell firing phase. In both cases, however, tufted cells fire systematically earlier than mitral cells. These findings suggest that mitral cells need more time to encode their responses in low odor molecule concentrations. Moreover, Gire et al. (2012) suggest that the more efficient direct excitation of tufted cells from olfactory sensory neurons makes them more suitable for coding for concentration compared to mitral cells. Our results suggest that the coding mechanism differs depending on the magnitude of the concentration. Comparing our results at very low concentrations (baseline x0.1 – 0.4) compared to higher concentrations (baseline x0.4 – 2) we observe a shift in the coding mechanisms (figures 4.16 - 4.20). Specifically, at lower concentrations both mitral and tufted cells (but especially tufted) seem to be encoding concentration in their firing latency. In higher concentrations, however, we observe a shift in the coding mechanism to the firing rate of both cells (especially tufted cells). At very high concentrations, where tufted cell firing seems to reach a plateau, firing rate of mitral cells is more suitable for coding for odor concentration.

5.3.2 Differentiating versus grouping of similar odors

Mitral cells exhibit a finer response to odor stimuli, defined by the lower firing probability and the extended lateral inhibition. Therefore, they are more suitable for coding for the identity of odor molecules. On the other hand, tufted cells are more easily excited and exhibit more robust responses. These features make them more suitable for the grouping of similar odors. This was evident in our results where mitral cells encoded similar odors with more separated spatial patterns (represented by the ensemble of coding neurons) compared to tufted cells whose response patterns where more overlapping (figures 4.24 - 4.27). This view is also supported by a recent study on the distinct modulation of mitral versus tufted cell firing response by serotoninergic inputs (Kapoor et al., 2016). In this study, they show that activation of neurons of raphe nuclei leads to sensitization of tufted cell response to odor stimuli, whereas it has a bidirectional modulatory effect in mitral cells. They conclude that raphe activation increases correlation of odor representations by the tufted encoding network (decoded by anterior region of the olfactory cortex) and decorrelation of odor representations (pattern separation) by the mitral encoding network (decoded by both anterior and posterior region of the olfactory cortex). Such mechanisms would enable the olfactory system to simultaneously extract information regarding grouping and differentiating of similar odors.

5.3.3 Encoding simple but vital versus demanding tasks

Mitral cells have been suggested to be recruited for the discrimination of odors during demanding tasks (Igarashi et al., 2012), which is in agreement with the longer time required for rodents to accurately discriminate similar odors. An interesting conclusion can be that tufted cells are the fast messengers conveying vital information, easy to discriminate that is required for reflex responses, for example during dangerous condition. Mitral cells on

the other hand, have been proposed to be the fine-tuners (Fukunaga et al., 2012) who at an early stage of the odor processing pathway refine the odor representation based on previously learned information.

6 | Conclusions - Future Work

In this study we investigated the possible mechanisms responsible for the distinct response properties of mitral and tufted cells of the olfactory bulb. We explored both single cell and network parameters and associated them with specific response properties. By systematically and individually modifying conductances of ionic channels we evaluated their contribution in shaping the response of principal neurons. However, given the simplified morphology of the models we used we did not conduct a systematic investigation of the effect of morphological parameters. Future studies, ideally using detailed morphological models, should explore the contribution of the different morphological properties in the response of mitral and tufted cells.

For our network simulations we used a model that includes the basic elements of the olfactory bulb. However, in reality, the complexity of the olfactory bulb circuit is much higher. Modelling of more realistic networks will be more computationally demanding and was out of the scope of this study. Such an approach also demands further information from experimental studies regarding the connectivity between local interneurons and principal neurons, that are currently unavailable. Given our current knowledge, it would be interesting to explore in future studies the effect of other network properties such as the indirect excitation of mitral cells from olfactory sensory neurons through local interneurons (possibly external tufted cells and short-axon cells) and the gap junctions that exist between principal neurons. What is more, it would be interesting to model and explore the effect of cortical and subcortical (cholinergic, serotonergic, adrenergic) modulatory inputs.

The final aim of our study was to investigate the functional role of the distinct subtypes of principal neurons. We studied the response patterns after stimulation with inputs representing increasing odor concentration or with similar input patterns representing similar odors. In future studies it would be in-

teresting to explore the responses of the parallel networks after stimulation with combinations of odor inputs representing odor mixtures and with odor inputs that change during the simulation representing evolving odor stimuli. All in all, studies of the olfactory system in general and of the olfactory bulb in particular have much to offer to our understanding of information processing mechanisms, considering the huge amount of different odors that these systems encode. In the end, they improve our knowledge of how our brains work.

Bibliography

Shawn D Burton and Nathaniel N Urban. Greater excitability and firing irregularity of tufted cells underlies distinct afferent-evoked activity of olfactory bulb mitral and tufted cells. *The Journal of physiology*, 592(10): 2097–2118, 2014.

S Cajal. Ramon: Histologie du système nerveux de l'homme et des vertébrés, vol. ii, a. *Maloine, Paris*, 1911.

Ryan M Carey, William Erik Sherwood, Michael T Shipley, Alla Borisyuk, and Matt Wachowiak. Role of intraglomerular circuits in shaping temporally structured responses to naturalistic inhalation-driven sensory input to the olfactory bulb. *Journal of Neurophysiology*, pages jn–00394, 2015.

Nicholas T Carnevale and Michael L Hines. *The NEURON book*. Cambridge University Press, 2006.

JM Christie, NE Schoppa, and GL Westbrook. Tufted cell dendrodendritic inhibition in the olfactory bulb is dependent on nmda receptor activity. *Journal of neurophysiology*, 85(1):169, 2001.

Thomas A Cleland and Christiane Linster. Computation in the olfactory system. *Chemical senses*, 30(9):801–813, 2005.

Andrew P Davison, Jianfeng Feng, and David Brown. Dendrodendritic inhibition and simulated odor responses in a detailed olfactory bulb network model. *Journal of neurophysiology*, 90(3):1921–1935, 2003.

Nicolas Fourcaud-Trocmé, Emmanuelle Courtiol, and Nathalie Buonviso. Two distinct olfactory bulb sublaminar networks involved in gamma and beta oscillation generation: a csd study in the anesthetized rat. *Frontiers in neural circuits*, 8, 2014.

Izumi Fukunaga, Manuel Berning, Mihaly Kollo, Anja Schmaltz, and Andreas T Schaefer. Two distinct channels of olfactory bulb output. *Neuron*, 75(2):320–329, 2012.

David H Gire, Kevin M Franks, Joseph D Zak, Kenji F Tanaka, Jennifer D Whitesell, Abigail A Mulligan, René Hen, and Nathan E Schoppa. Mitral cells in the olfactory bulb are mainly excited through a multistep signaling path. *The Journal of Neuroscience*, 32(9):2964–2975, 2012.

Edwin R Griff, Mariam Mafhouz, and Michel A Chaput. Comparison of identified mitral and tufted cells in freely breathing rats: Ii. odor-evoked responses. *Chemical senses*, 33(9):793–802, 2008.

Stephen Grossberg. Beta oscillations and hippocampal place cell learning during exploration of novel environments. *Hippocampus*, 19(9):881–885, 2009.

Lewis B Haberly and Joseph L Price. The axonal projection patterns of the mitral and tufted cells of the olfactory bulb in the rat. *Brain research*, 129 (1):152–157, 1977.

Abdallah Hayar, Sergei Karnup, Matthew Ennis, and Michael T Shipley. External tufted cells: a major excitatory element that coordinates glomerular activity. *The Journal of neuroscience*, 24(30):6676–6685, 2004.

Kei M Igarashi, Nao Ieki, Myungho An, Yukie Yamaguchi, Shin Nagayama, Ko Kobayakawa, Reiko Kobayakawa, Manabu Tanifuji, Hitoshi Sakano, Wei R Chen, et al. Parallel mitral and tufted cell pathways route distinct odor information to different targets in the olfactory cortex. *The Journal of Neuroscience*, 32(23):7970–7985, 2012.

Fumiaki Imamura, Hiroshi Nagao, Hiromi Naritsuka, Yasunobu Murata, Hisaaki Taniguchi, and Kensaku Mori. A leucine-rich repeat membrane

protein, 5t4, is expressed by a subtype of granule cells with dendritic arbors in specific strata of the mouse olfactory bulb. *Journal of Comparative Neurology*, 495(6):754–768, 2006.

Bernhard A Kaplan and Anders Lansner. A spiking neural network model of self-organized pattern recognition in the early mammalian olfactory system. *Front. Neural Circuits*, 8(5):10–3389, 2014.

Vikrant Kapoor, Allison C Provost, Prateek Agarwal, and Venkatesh N Murthy. Activation of raphe nuclei triggers rapid and distinct effects on parallel olfactory bulb output channels. *Nature neuroscience*, 2016.

Leslie M Kay, Jennifer Beshel, Jorge Brea, Claire Martin, Daniel Rojas-Líbano, and Nancy Kopell. Olfactory oscillations: the what, how and what for. *Trends in neurosciences*, 32(4):207–214, 2009.

Shu Kikuta, Max L Fletcher, Ryota Homma, Tatsuya Yamasoba, and Shin Nagayama. Odorant response properties of individual neurons in an olfactory glomerular module. *Neuron*, 77(6):1122–1135, 2013.

Thomas Klausberger, Peter J Magill, László F Márton, J David B Roberts, Philip M Cobden, György Buzsáki, and Peter Somogyi. Brain-state-and cell-type-specific firing of hippocampal interneurons in vivo. *Nature*, 421 (6925):844–848, 2003.

David Kleinfeld, Martin Deschênes, and Nachum Ulanovsky. Whisking, sniffing, and the hippocampal?-rhythm: A tale of two oscillators. *PLoS Biol*, 14(2):e1002385, 2016.

Alexei A Koulakov and Dmitry Rinberg. Sparse incomplete representations: a potential role of olfactory granule cells. *Neuron*, 72(1):124–136, 2011.

Guoshi Li and Thomas A Cleland. A two-layer biophysical model of cholinergic neuromodulation in olfactory bulb. *The Journal of Neuroscience*, 33 (7):3037–3058, 2013.

Claudia Lodovichi, Leonardo Belluscio, and Lawrence C Katz. Functional topography of connections linking mirror-symmetric maps in the mouse olfactory bulb. *Neuron*, 38(2):265–276, 2003.

Foteos Macrides, Thomas A Schoenfeld, James E Marchand, and Andrew N Clancy. Evidence for morphologically, neurochemically and functionally heterogeneous classes of mitral and tufted cells in the olfactory bulb. *Chemical Senses*, 10(2):175–202, 1985.

Florian T Merkle, Luis C Fuentealba, Timothy A Sanders, Lorenza Magno, Nicoletta Kessaris, and Arturo Alvarez-Buylla. Adult neural stem cells in distinct microdomains generate previously unknown interneuron types. *Nature neuroscience*, 17(2):207–214, 2014.

K. Mori. *The Olfactory System: From Odor Molecules to Motivational Behaviors*. Springer, 2014. ISBN 9784431543770. URL `https://books.google.gr/books?id=Qcr8sgEACAAJ`.

Kensaku Mori and Hitoshi Sakano. How is the olfactory map formed and interpreted in the mammalian brain? *Annual review of neuroscience*, 34: 467–499, 2011.

Shin Nagayama, Yuji K Takahashi, Yoshihiro Yoshihara, and Kensaku Mori. Mitral and tufted cells differ in the decoding manner of odor maps in the rat olfactory bulb. *Journal of neurophysiology*, 91(6):2532–2540, 2004.

Shin Nagayama, Allicia Enerva, Max L Fletcher, Arjun V Masurkar, Kei M Igarashi, Kensaku Mori, and Wei R Chen. Differential axonal projection of mitral and tufted cells in the mouse main olfactory system. *Frontiers in neural circuits*, 4, 2010.

Shin Nagayama, Ryota Homma, and Fumiaki Imamura. Neuronal organization of olfactory bulb circuits. *Frontiers in Neural Circuits*, 8:98, 2014.

Marion Najac, Didier De Saint Jan, Leire Reguero, Pedro Grandes, and Serge Charpak. Monosynaptic and polysynaptic feed-forward inputs to mitral cells from olfactory sensory neurons. *The Journal of Neuroscience*, 31(24):8722–8729, 2011.

Edward Orona, Elizabeth C Rainer, and John W Scott. Dendritic and axonal organization of mitral and tufted cells in the rat olfactory bulb. *Journal of Comparative Neurology*, 226(3):346–356, 1984.

Davide Polese, Eugenio Martinelli, Santiago Marco, Corrado Di Natale, and Agustin Gutierrez-Galvez. Understanding odor information segregation in the olfactory bulb by means of mitral and tufted cells. *PloS one*, 9(10): e109716, 2014.

Masayuki Sakamoto, Ryoichiro Kageyama, and Itaru Imayoshi. The functional significance of newly born neurons integrated into olfactory bulb circuits. *Frontiers in neuroscience*, 8, 2014.

Gordon M Shepherd, WR Chen, and CA Greer. *The synaptic organization of the brain*. Oxford University Press New York, 2004.

Roman Shusterman, Matthew C Smear, Alexei A Koulakov, and Dmitry Rinberg. Precise olfactory responses tile the sniff cycle. *Nature neuroscience*, 14(8):1039–1044, 2011.

Naoshige Uchida, Cindy Poo, and Rafi Haddad. Coding and transformations in the olfactory system. *Annual review of neuroscience*, 37:363–385, 2014.

Justus V Verhagen, Daniel W Wesson, Theoden I Netoff, John A White, and Matt Wachowiak. Sniffing controls an adaptive filter of sensory input to the olfactory bulb. *Nature neuroscience*, 10(5):631–639, 2007.

Matt Wachowiak and Michael T Shipley. Coding and synaptic processing of sensory information in the glomerular layer of the olfactory bulb. In *Sem-*

inars in cell & developmental biology, volume 17, pages 411–423. Elsevier, 2006.

Yuguo Yu, Thomas S McTavish, Michael L Hines, Gordon M Shepherd, Cesare Valenti, and Michele Migliore. Sparse distributed representation of odors in a large-scale olfactory bulb circuit. *PLoS Comput Biol*, 9(3): e1003014, 2013.